
An Empirical Study of Assumptions in Bayesian Optimisation

Alexander I. Cowen-Rivers^{*1} Wenlong Lyu^{*1} Rasul Tutunov^{*1} Zhi Wang¹ Antoine Grosnit¹
 Ryan Rhys Griffiths² Hao Jianye¹ Jun Wang¹³ Haitham Bou Ammar¹⁴

Abstract

Inspired by the increasing desire to efficiently tune machine learning hyper-parameters, in this work we rigorously analyse conventional and non-conventional assumptions inherent to Bayesian optimisation. Across an extensive set of experiments we conclude that: 1) the majority of hyper-parameter tuning tasks exhibit heteroscedasticity and non-stationarity, 2) multi-objective acquisition ensembles with Pareto-front solutions significantly improve queried configurations, and 3) robust acquisition maximisation affords empirical advantages relative to its non-robust counterparts. We hope these findings may serve as guiding principles, both for practitioners and for further research in the field.

1. Introduction

Although achieving significant success in numerous applications (Bobadilla et al., 2013; Litjens et al., 2017; Fatima & Pasha, 2017; Kandasamy et al., 2018; Cowen-Rivers et al., 2020), the performance of machine learning models chiefly depends on the correct setting of hyper-parameters. As models grow larger and more complex, efficient and autonomous hyper-parameter tuning algorithms become crucial determinants of performance. To this end, a variety of methods from black-box and multi-fidelity optimisation have been adopted (Kandasamy et al., 2017; Sen et al., 2018) with varying degrees of success. Techniques such as Bayesian optimisation (BO), for example, enable sample efficiency (in terms of black-box evaluations) at the expense of high computational demands, while “unguided” bandit-based approaches can fail to converge (Falkner et al., 2018). Identifying such failure modes, the authors in (Falkner et al., 2018) built on (Li et al., 2017) to propose a combination of

bandits and BO that achieves the best of both worlds; fast convergence and computational scalability. Though impressive, such successes of BO and alternatives, conceal a set of restrictive modelling and acquisition function assumptions that are hindering the widespread adoption of BO. We begin by describing these assumptions.

Modelling Assumptions: Critical to BO performance is a set of data modelling assumptions that admit an effective probabilistic model of the true black-box objective (e.g., validation loss in hyper-parameter tuning tasks). This model should not only provide accurate point estimates, but should also maintain calibrated uncertainty estimates to guide exploration of the objective. Amongst many possible surrogates (Springenberg et al., 2016; Hutter et al., 2011), Gaussian processes (GPs) are the default choice due to their flexibility and sample efficiency. Growing interest in applications of Bayesian optimisation has catalysed significant engineering feats enhancing the scalability and training efficiency of GP surrogates by exploiting graphical processing units (Knudde et al., 2017; Balandat et al., 2020).

Similar to any other framework, the correct specification of a GP model is dictated by the data modelling assumptions imposed by the user. For instance, a homoscedastic GP suffers when asked to model data with heteroscedastic noise whilst stationary GPs fail to track non-stationary targets. Of course, the aforementioned shortcomings are not unnatural in real-world problems but arise precisely in tasks related to hyper-parameter tuning of machine learning algorithms as depicted in our tests in Section 3.1. Hence, even if one improves computational efficiency, commonly-made assumptions such as homoscedasticity and stationarity may easily hinder any tuning algorithm’s performance. Despite the importance of these assumptions in practice, GPs that presume homoscedasticity and stationarity are typically taken at face value and implemented as is.

Acquisition Function & Optimiser Assumptions: Modelling choices like those mentioned above are not unique to the fitting procedure but rather transcend to other pivotal steps of hyper-parameter tuners. Precisely, given a model that adheres to some (or all) assumptions mentioned above, the second step involves maximising an acquisition function to query novel input locations that are then evalu-

^{*}Equal contribution ¹Huawei R&D London ²Work completed during an internship at Huawei R&D London ³University College London ⁴Honorary position at University College London. Correspondence to: Alexander I. Cowen-Rivers <alexander.cowen.rivers@huawei.com>.

ated. Hence, practitioners introduce additional constraints relating to the category of optimisation variables and the choice of acquisitions. When it comes to variable types, main-stream implementations (Knudde et al., 2017; Balandat et al., 2020) assume continuous domains and employ first and second-order optimisers e.g., LBFGS (Liu & Nocedal, 1989) and ADAM (Kingma & Ba, 2015) to determine queried points. Real-valued configurations cover but a subset of possible machine learning hyper-parameters rendering discrete types, like hidden layer size in deep networks, out of scope. Moreover, from the point of view of acquisition functions, libraries tend to presuppose that one unique acquisition performs best in a given task, limiting benefits that can arise from a combined solution as we demonstrate in Section 5.

Contributions: Having identified essential modelling choices in BO, our goal in this paper is to provide empirical insight into their effect on experimental performance with the aim of informing the community on best practices for hyper-parameter tuning. We wish for our findings to apply to a broad array of tasks and datasets, be attentive to the effect of random initialisation on algorithmic performance, and naturally, be reproducible. As such, we prefer to build on already established benchmark packages, especially those that enable fast and scalable evaluations sanctioning multi-seeding protocols. To that end, we undertake our evaluation in 2140 experiments from 108 real-world problems from the UCI repository (Dua & Graff, 2017), which also featured as a testbed in the NeurIPS 2020 black-box optimisation challenge. Our empirical findings point towards the following conclusions:

1. Hyper-parameter tuning of machine learning tasks exhibit significant levels of heteroscedasticity and non-stationarity;
2. Applying input-warping and output transformation mitigates these effects giving rise to more well-behaved tuners with higher mean, and median performance across all 108 black-box functions under examination;
3. Individual acquisition functions tend to conflict in their solution (i.e., an optimum for one can be a bad point for the other and vice versa). Using a multi-objective formulation significantly improves performance;
4. Targeting robust formulations of acquisitions admit better tuners.

To further solidify our conclusions, we conducted additional ablation studies, realising a ranked order of importance in significant components. We found that input and output warping (conclusion 2) and multi-objective acquisitions (conclusion 3) led to the most significant improvements followed by the robustness of acquisitions (conclusion 4).

2. Standard Design Choices in BO

As discussed earlier, the problem of hyper-parameter tuning can be framed as an instance of black-box optimisation:

$$\arg \max_{\mathbf{x} \in \mathcal{X}} f(\mathbf{x}), \quad (1)$$

with \mathbf{x} denoting a configuration choice, \mathcal{X} a (potentially) mixed design space, and $f(\mathbf{x})$ a validation accuracy we wish to maximise.

In this paper, we focus on BO as a solution concept for black-box problems of the form depicted in Equation 1. BO considers a sequential decision approach to the global optimisation of a function $f : \mathcal{X} \rightarrow \mathbb{R}$ over a bounded input domain \mathcal{X} . At each decision round, i , the algorithm selects a collection of q inputs $\mathbf{x}_{1:q}^{(new)} \in \mathcal{X}^q$ and observes values of the *black-box* function $\mathbf{y}_{1:q}^{(new)} = f(\mathbf{x}_{1:q}^{(new)})$. The goal is to rapidly approach the maximum $\mathbf{x}^* = \arg \max_{\mathbf{x} \in \mathcal{X}} f(\mathbf{x})$. Since both $f(\cdot)$ and \mathbf{x}^* are unknown, solvers need to trade off exploitation and exploration during this search process.

To achieve this goal, BO algorithms operate in two steps. In the first, a Bayesian model is learned, while in the second an acquisition function determining new query locations is maximised. Next, we survey frequently-made assumptions in mainstream BO implementations and contemplate their implications on performance.

2.1. Modelling Assumptions

When black-boxes are real-valued, Gaussian process regression (Rasmussen & Williams, 2006) are effective surrogates due to their flexibility and ability to maintain calibrated uncertainty estimates. In established implementations of BO, designers place GP priors on latent functions, $f(\cdot)$, which are fully specified through a mean function, $m(\mathbf{x})$, and a covariance function or kernel $k_{\theta}(\mathbf{x}, \mathbf{x}')$ with θ representing kernel hyper-parameters. The model specification is completed by defining a likelihood. Here, practitioners typically assume that observations y_l adhere to a Gaussian noise model such that $y_l = f(\mathbf{x}_l) + \epsilon_l$ where $\epsilon_l \sim \mathcal{N}(0, \sigma_{\text{noise}}^2)$. This, in turn, generates a Gaussian likelihood of the form $y_l | \mathbf{x}_l \sim \mathcal{N}(f_l, \sigma_{\text{noise}}^2)$ where we use f_l to denote $f(\mathbf{x}_l)$ with $f(\mathbf{x}) \sim \mathcal{GP}(m(\mathbf{x}), k_{\theta}(\mathbf{x}, \mathbf{x}'))$. Additionally, a further design choice commonly made by practitioners is that the GP kernel is stationary, depending only on the norm between \mathbf{x} and \mathbf{x}' , $\|\mathbf{x} - \mathbf{x}'\|$. From this exposition, we conclude two important modelling assumptions stated as *data stationarity* and *homoscedasticity of the noise distribution*. If the true latent process does not adhere to these assumptions, the resultant model will be a poor approximation to the black-box. Realising the potential empirical effects of these modelling choices, we identify the first two questions of this paper:

Q.I. Are parameter tuning tasks stationary and homoscedastic ?

Q.II. How do inexact modelling assumptions effect BO performance ?

In Section 3.1, we show that even the simplest among machine learning tasks pass tests of heteroscedasticity and non-stationarity and that overlooking such factors (Section 3.2) can quickly deteriorate performance.

2.2. Acquisitions & Optimisation Assumptions

Acquisition functions trade off exploration and exploitation by utilising statistics from the posterior $p_{\theta}(f(\cdot)|\mathcal{D})$ with \mathcal{D} denoting data (parameter configurations as inputs and validation accuracy as outputs) collected so far. Under a GP surrogate, such a posterior is Gaussian itself. To simplify the exposition, we defer the exact equations to Appendix C.1 and just note that $p(f(\mathbf{x}_{1:q})|\mathcal{D}) = \mathcal{N}(\boldsymbol{\mu}_{\theta}(\mathbf{x}_{1:q}), \boldsymbol{\Sigma}_{\theta}(\mathbf{x}_{1:q}))$. In this paper, we focus on three widely-used myopic acquisition functions which in a reparameterised form can be written as (Wilson et al., 2017):

Expected improvement (EI):

$$\alpha_{\text{EI}}^{\theta}(\mathbf{x}_{1:q}|\mathcal{D}) = \mathbb{E}_{\text{post.}} \left[\max_{j \in 1:q} \{\text{ReLU}(f(\mathbf{x}_j) - f(\mathbf{x}^+))\} \right],$$

where the subscript post. is the predictive posterior of a GP (Rasmussen & Williams, 2006), \mathbf{x}_j is the j^{th} vector of $\mathbf{x}_{1:q}$, and \mathbf{x}^+ is the best performing input in the data so far.

Probability of improvement (PI):

$$\alpha_{\text{PI}}^{\theta}(\mathbf{x}_{1:q}|\mathcal{D}) = \mathbb{E}_{\text{post.}} \left[\max_{j \in 1:q} \{\mathbb{1}\{f(\mathbf{x}_j) - f(\mathbf{x}^+)\}\} \right],$$

where $\mathbb{1}\{\cdot\}$ is the left-continuous Heaviside step function.

Upper confidence bound (UCB):

$$\alpha_{\text{UCB}}^{\theta}(\mathbf{x}_j) = \mathbb{E}_{\text{post.}} \left[\max_{j \in 1:q} \left\{ \mu_{\theta}(\mathbf{x}_j) + \sqrt{\beta\pi/2} |\gamma_{\theta}(\mathbf{x}_j)| \right\} \right],$$

where $\mu_{\theta}(\mathbf{x}_j)$ is the posterior mean of the predictive distribution and $\gamma_{\theta}(\mathbf{x}_j) = f(\mathbf{x}_j) - \mu_{\theta}(\mathbf{x}_j)$.

When it comes to practicality, generic BO implementations make additional assumptions during the acquisition maximisation step. First, it is assumed that one of the aforementioned acquisitions works best for a specific task, and that the GP model is an accurate approximation to the black-box. However, when it comes to real-world applications, both of these assumptions are hard to validate; the best-performing acquisition is challenging to identify up-front and GP models can easily be misspecified. With this in mind, we identify a further question that we wish to answer:

Q.III. Can acquisition function solutions conflict in hyper-parameter tuning tasks ?

In the next section, we affirm that acquisitions can conflict even on the simplest of machine learning tasks. Moreover, we show that a robust formulation to tackle misspecification of acquisition maximisation can improve overall performance (see Section 4.2.1).

3. Data Analysis & Question Answering

Before proceeding to potential improvements to BO, we now detail several tests we conducted to answer the questions (Q.I., Q.II., and Q.III.) posed in the previous section. Our analysis indicates:

(A.I. Answer to Q.I.): Even simple machine learning tasks exhibit significant heteroscedasticity and non-stationarity.

A.II. (Answer to Q.II.): Inexact modelling assumptions significantly hurt BO, costing mean performance ca. 3% and lower percentiles ca. 4%.

A.III. (Answer to Q.III.): Acquisition functions conflict in their optima, occasionally leading to opposing solutions.

Experimental Setting: We create a wide range of hyper-parameter tasks problems across a variety of classification and regression problems. It contains nine models including but not limited to multi-layer perceptrons, decision trees, random forests, and support-vector machines, six datasets (two regression and four classification) from the UCI repository, and two metrics per dataset such as negative log-likelihood or mean squared error. Each of the models possesses tuneable hyper-parameters, e.g., the regularisation constant of a support-vector machine, or the number of units of a neural network. The goal is to fit those hyper-parameters so as to maximise/minimise one of the metrics previously mentioned. Of course, such black-box values are stochastic with randomness originating from various sources, e.g., train-test splits to compute validation losses, and random seeds of optimisation algorithms. Experimentation was facilitated by the Bayesmark packaged.

As a solver, we wish to adopt BO but note that we also experimented with other approaches such as HyperOpt (Bergstra et al., 2015). Our findings in Section 5 demonstrate that a Bayesian optimiser with improved design choices can achieve state-of-the-art results on these tasks.

3.1. Answer A.I.: Simple Tasks are Complex

To provide answers to Q.I., we run tests for heteroscedasticity and non-stationarity. Each of these tests is run on every task combination (i.e., model, data, metric) with 50 unique hyper-parameters. We repeat each ten folds while fixing the hyper-parameter configuration.

Heteroscedasticity Tests: To gauge heteroscedasticity, we use Fligner and Killeen (Fligner & Killeen, 1976) and Lev-

ene (Levene, 1960) tests. It was shown in (Conover et al., 1981) that both these tests are reliable in terms of robustness to departures from normality (Park & Lindsay, 1999). Both test the null hypothesis that the underlying black-box function (e.g., validation accuracy (**hyper-parameter**_{*i*})) is homoscedastic. In all 108 tests, we see a p-value significantly lower than 0.05 in 72 tasks using Levene’s test, and in 73 tasks using Fligner and Killeen. Such results (shown in detail in Appendix B) imply that at least 66% of the experimental tasks exhibit heteroscedastic behaviour. Additionally, Figure 6 illustrates the heteroscedasticity of several tasks showing drastic changes of the observed noise level around the mean validation accuracy (**hyper-parameter**_{*i*}) for varying values of hyper-parameter.

Non-Stationarity Assessment: To test for non-stationarity we compare the fit of a vanilla Gaussian Process surrogate model equipped with a stationary kernel (Matern32) to a non-stationary kernel (Spectral Mixture). We took 32 unique hyper-parameters and their respective evaluation score for training and 32 for held-out testing. Over 108 tasks, averaged over five random seeds, we see in $\approx 30\%$ of tasks that the non-stationary kernel offers significantly better log probability on the held-out test set vs the stationary kernel, implicitly suggesting that handling non-stationarity is beneficial for the GP surrogate. See Table 4 in the Appendix for detailed results.

3.2. Answers A.II.: Modelling Assumptions Matter

In answer to **Q.II.**, we offer a first indication that data modelling assumptions matter through a comparison of approaches affording progressively better-specified models for black-box objectives. We evaluate a simple random search strategy along with four BO methods. These algorithms serve a dual-purpose as the set of baselines against which we compare our solution in section 5. SkOpt (Pedregosa et al., 2011) utilises homoscedastic, non-stationary GPs, HyperOpt (Bergstra et al., 2015) and BOHB (Falkner et al., 2018) allow for some relaxation of the assumptions of SkOpt whilst TuRBO (Eriksson et al., 2019b) employs local modelling capable of mitigating against the effects of heteroscedasticity and non-stationarity.

We consider 108 task combinations and apply standard batch BO for 16 iterations while generating 8 query points per BO step. We repeat each task across 20 random seeds amounting to 2140 experiments. To gauge performance, we use the normalised task score (as detailed in Appendix 3) to compare across tasks. We hypothesise that as modelling assumptions increase in sophistication, we would improve our modelling capabilities and improve performance, validated by Figure 1 with TuRBO performing best at around 6% improvement in mean normalised score compared to random search. We attribute this to the fact that TuRBO uses the most advanced

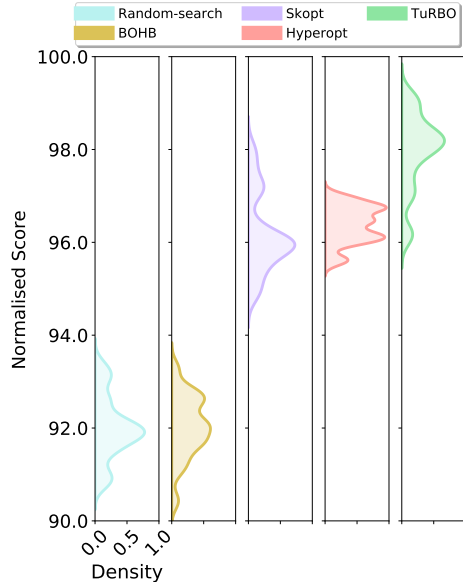


Figure 1. Density of normalised scores relative to random search.

modelling assumptions amongst tested algorithms. Having local models appears to reduce the effects of heteroscedasticity and non-stationarity. BOHB tended to underperform in our experiment, which we attribute to the fact that BOHB was designed explicitly for multi-fidelity optimisation in deep networks focusing on computational time reduction without explicit support for the batch BO setting.

In Section 5, we further highlight the importance of modelling choices by demonstrating that models capable of specifying heteroscedastic noise and non-stationary latent functions can achieve an additional 3% gain in mean and high quantiles and up to 4% increase in low normalised score quantiles.

3.3. Answer A.III.: A No Clear Winner

To answer **Q.III.** of whether acquisition functions can conflict in their solutions, we collect 32 samples from each task by evaluating various hyper-parameter configurations across different metrics. We then gather a dataset $\mathcal{D} = \{\mathbf{hyper-param}_i, y_i\}_{i=1}^{32}$, where **hyper-param**_{*i*} is a vector whose dimensionality depends on the number of hyper-parameters in a given model, and y_i corresponds to an evaluation metric, e.g., mean squared error (**hyper-param**_{*i*}). We then fit a GP surrogate model and consider each of the three acquisitions from Section 2.2. We visualise all three acquisition functions per hyperparameter dimension and report partial results in Figure 2 with a full set presented in Appendix D. From Figure 2, we realise that in some instances, acquisition functions not only provide different solutions, but those solutions can in fact conflict. To elaborate consider the Wine dataset using an AdaBoost model (i.e., left figure in 2). Here, a PI acquisition function deems

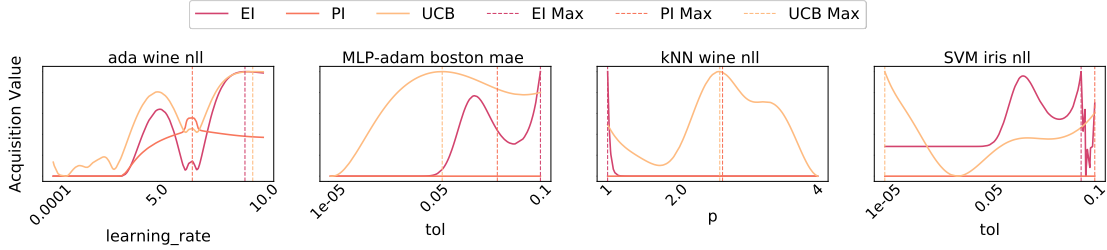


Figure 2. Examples depicting conflicting acquisitions across varying datasets (Wine, Boston Housing, and Iris) and models (AdaBoost, Multi-Layer perceptron, K-Nearest neighbours, and support vector machines).

a value of 6 for the learning rate as optimal, while EI considers that same value as an unlikely solution. It is worth noting that a learning rate in an AdaBoost model weighs ensemble estimators’ contribution rather than directly dictating the descent direction, thus explaining large domain values.

4. Optimising Bayesian Optimisation

Now, we elaborate on more general design choices that prove empirically effective. Some of the forthcoming remedies have been proposed elsewhere in settings beyond BO, while acquisition function robustness is unique to this work.

4.1. Tackling Heteroscedasticity and Non-Stationarity

To enable flexible modelling solutions capable of handling heteroscedasticity and non-stationarity, we apply ideas from the warped GP literature (Snelson et al., 2004) where output transformations allow for more complex noise processes. We found that the Box-Cox (Box & Cox, 1964) and Yeo-Johnson (Yeo & Johnson, 2000) output transformations and a Kumaraswamy (Kumaraswamy, 1980) input warping offered a balance of simplicity in implementation and empirical performance. In fact, in our ablation study (Section 5), we demonstrate that the addition of these two modelling components resulted in the largest performance gain.

Output Transformation for Heteroscedasticity: We consider the Box-Cox transformation typically used to map non-Gaussian data closer to “Gaussianity”. The class of transforms depend on a tuneable parameter ζ and apply the following map to each of the labels: $T_\zeta(y_l) = y_l^\zeta - 1/\zeta$ for $\zeta \neq 0$ and $T_\zeta(y_l) = \log y_l$ if $\zeta = 0$, where in our case y_l denotes a validation accuracy of the l^{th} hyper-parameter configuration. Of course, ζ has to be fit based on the observed data such that the distribution of the transformed labels closely resembles a Gaussian. This is achieved by minimising the negative of the Box-Cox likelihood function:

$$\log \left[\sum_{l=1}^n \frac{(T_\zeta(y_l) - \bar{T}_\zeta(\mathbf{y}))^2}{n} \right]^{\frac{n}{2}} + \sum_{l=1}^n \log [T_\zeta(y_l)]^{(1-\zeta)},$$

where n is the number of datapoints and $\bar{T}_\zeta(\mathbf{y})$ is the sample mean of the transformed labels. Of course, Box-Cox transforms only considers strictly positive (or strictly negative) labels y_l . To handle a more general setting, we also make use of the Yeo-Johnson transform (Yeo & Johnson, 2000). Due to space constraints we defer the details to Appendix C.2.

An important property we also considered when proposing such transformations is ease of implementation. For both transforms mentioned above, efficient implementations are readily available in various libraries such as Scikit-learn (Pedregosa et al., 2011) within the PowerTransform package where the Brent optimiser (Brent, 2013) is used for determining ζ^* .

Input Transformations for Non-Stationarity: Having dealt with heteroscedasticity, now we shift our attention to tackle data non-stationarity. As a general solution concept, we consider input warping see (Snoek et al., 2012). In our implementation, we relied on a Kumaraswamy input warping, which executes the following for each of the input dimensions:

$$[\text{Kumaraswamy}_\gamma(\mathbf{x}_l)]_k = 1 - (1 - [\mathbf{x}_l]_k^{a_k})^{b_k} \quad \forall k \in [1 : d],$$

with d being the dimensionality of the decision variable (e.g., number of free hyper-parameters), a_k and b_k are tuneable warping parameters for each of the dimensions, and γ is a vector concatenating all free parameters, i.e., $\gamma = [a_{1:d}, b_{1:d}]^T$. Of course, γ is fit based on observed data. Similar to (Balandat et al., 2020), we consider γ as part parameters of the marginal likelihood that we optimise while fitting our GP.

All Modelling Improvements Together: Combining the above considerations of heteroscedasticity and non-stationarity leads us to an improved GP model with more flexible capabilities. The implementation of such a model is relatively simple and involves maximising a new marginal that can be written as:

$$\max_{\theta, \gamma} - \frac{1}{2} \mathbf{T}_{\zeta^*}(\mathbf{y})^\top (\mathbf{K}_\theta^\gamma + \sigma_{\text{noise}} \mathbf{I})^{-1} \mathbf{T}_{\zeta^*}(\mathbf{y}) - \frac{1}{2} |\mathbf{K}_\theta^\gamma + \sigma_{\text{noise}}^2 \mathbf{I}| - \text{const},$$

where θ are GP hyper-parameters, γ corresponds to non-stationary transforms, and ζ^* denotes the solution to a `Box-Cox` likelihood objective. It is worth noting that we used `Box-Cox` as a running example but as mentioned previously we interchange `Box-Cox` with `Yeo-Johnson` transforms based on the properties of the label y_i . Moreover, we used $\mathbf{K}_\theta^\gamma \in \mathbb{R}^{n \times n}$ to represent a matrix such that each entry depends on both θ and γ , where $k_\theta^\gamma(\mathbf{x}, \mathbf{x}') = k_\theta(\text{Kumaraswamy}_\gamma(\mathbf{x}), \text{Kumaraswamy}_\gamma(\mathbf{x}'))$.

4.2. Tackling Acquisition Conflict & Robustness

Having proposed modifications to the modelling process of BO, we now concentrate on the acquisition maximisation step. In particular, we handle two problems, one related to the assumption of a perfect GP surrogate, with the second centred around conflicting acquisitions.

4.2.1. A ROBUST ACQUISITION OBJECTIVE

As mentioned in Section 2.2, the acquisition maximisation step assumes that adequate surrogates are readily available. Especially during early rounds of training, such a property is hard to validate as data is scarce leading to (sometimes) severe model misspecification that hurts performance. One way to tackle such a problem is to assume a robust formulation (Kirschner et al., 2020; Klein et al., 2017) that attempts to find the best performing query location under the worst-case GP model, i.e., solving $\max_{\mathbf{x}} \min_{\theta} \alpha^\theta(\mathbf{x}|\mathcal{D})$. Granted such a formulation allows for a solution \mathbf{x}^* that is robust to worst-case misspecification in θ , having a max min acquisition is troubling for several reasons. From a conceptual perspective max min formulations are known to lead to very conservative solutions if not correctly constrained or regularised since the optimiser possesses the power to impair the GP fit while updating θ ¹. From an implementation perspective, one faces two further issues. First, no global convergence guarantees are known for the non-convex non-concave case that we face (Lin et al., 2020), and second, ensuring gradients can propagate through the computation graph restrict surrogates and acquisition functions to be within the same programming framework.

To avoid worst-case solutions and enable independence between acquisition functions and surrogate models, we borrow ideas from domain randomisation (Tobin et al., 2017) and consider an expected formulation instead: $\max_{\mathbf{x}} \alpha_{\text{rob}}(\cdot) \equiv \max_{\mathbf{x}} \mathbb{E}_{\epsilon \sim \mathcal{N}(0, \sigma_\epsilon^2 \mathbf{I})} [\alpha^{\theta+\epsilon}(\mathbf{x}|\mathcal{D})]$. Importantly, this problem seeks to find new query locations that perform well on average over a distribution of surrogate

¹Of course, one can argue augmenting the objective with a constraint such that θ updates remain close to θ^* of the marginal. The value by which such proximity needs to be enforced remains unclear in robust literature to date (Abdullah et al., 2019; Kirschner et al., 2020).

models rather than assuming a perfect surrogate.

Though appealing, our formulation still assumes access to the GP’s hyper-parameters, complicating implementation and restricting models and optimisers to the same programming paradigm. We wish to enable robustness by only having access to the GP’s mean and variance predictions for simplicity. Fortunately, we are able to show that upon a simple acquisition perturbation one can approximate the above $\alpha_{\text{rob}}(\cdot)$. Namely, we prove (see Appendix C) that if $\bar{\alpha}^\theta(\mathbf{x}|\mathcal{D}) = \alpha^\theta(\mathbf{x}|\mathcal{D}) + \eta\sigma_n$ with $\eta \sim \mathcal{N}(0, 1)$, then upon further technical details² we have (with high probability):

$$|\bar{\alpha}^\theta(\mathbf{x}|\mathcal{D}) - \mathbb{E}_{\epsilon \sim \mathcal{N}(0, \sigma_\epsilon^2 \mathbf{I})} [\alpha^{\theta+\epsilon}(\mathbf{x}|\mathcal{D})]| \leq \rho,$$

for any arbitrary $\rho \in (0, 1)$.

The bound above enables uncomplicated yet effective, robust implementations. For instance, if we would like to “robustify” a UCB acquisition, we add $\eta\sigma_n$ to the posterior’s mean and follow standard UCB onwards.

4.2.2. MULTI-OBJECTIVE ACQUISITIONS

As a final component of our general framework, we propose the usage of multi-objective acquisitions and seek a Pareto-front solution concept. This formulation enables a form of “hedging” between different acquisitions such that any other acquisition does not dominate the solution, thus representing the best solution trade-off (Lyu et al., 2018). Formally, we solve:

$$\max_{\mathbf{x}} (\bar{\alpha}_{\text{EI}}^\theta(\mathbf{x}|\mathcal{D}), \bar{\alpha}_{\text{PI}}^\theta(\mathbf{x}|\mathcal{D}), \bar{\alpha}_{\text{UCB}}^\theta(\mathbf{x}|\mathcal{D})), \quad (2)$$

where $\bar{\alpha}_{\text{type}}^\theta(\mathbf{x}|\mathcal{D})$ is a robust acquisition as introduced in the previous section and $\text{type} \in \{\text{EI}, \text{PI}, \text{UCB}\}$. We also note that our formulation is meant to reflect the fact of using a robust objective value of $\bar{\alpha}^\theta(\mathbf{x}|\mathcal{D}) = \alpha^\theta(\mathbf{x}|\mathcal{D}) + \eta_k\sigma_n$ with η_k being a sample from $\mathcal{N}(0, 1)$ at each iteration of the evolutionary solver.

Although solving the problem in Equation 2 is a formidable challenge, we note the existence of many mature multi-objective optimisation algorithms. These range from first-order (Kingma & Welling, 2014) to zero-order (Loshchilov & Hutter, 2016; Gabillon et al., 2020) and evolutionary methods (Hansen, 2016; Deb et al., 2002). Due to the discrete nature of hyper-parameters in machine learning tasks, we advocate using evolutionary solvers that naturally handle categorical and integer-valued variables. In our experiments, we employ the non-dominated sorting genetic algorithm II (NSGA-II) that allows for mixed variable crossover and

²We would like to mention that though a gradient-based algorithm remains intact upon the addition of $\eta\sigma_n$, in our formulation we use an evolutionary method which utilises acquisition function values. Consequently, the path followed by the optimiser will be altered based on η samples leading to more robust probes.

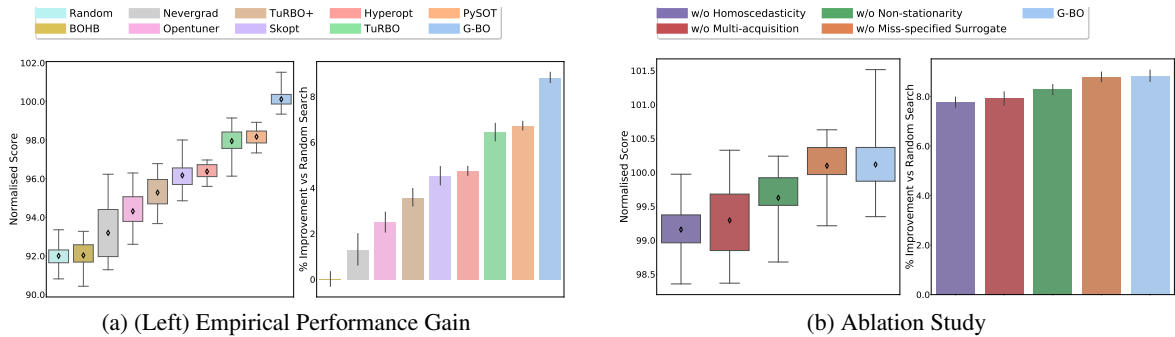


Figure 3. Analysis of the results on 108 tuning tasks. (a-Left) Normalised score comparison demonstrating that G-BO (i.e., BO with improvements from Section 4) outperforms others. (a-Right) Empirical gain demonstrating that G-BO can arrive at 8% improvement compared to random. (b-Left) Ablation study reflecting the importance of each addition. (b-Right) Gains associated with each step in % improvement compared to random search.

mutation to optimise real and integer input types (Deb et al., 2002). Importantly, an available stable implementation of NSGA-II along with other solvers can be found in the latest release of PyMOO (Blank & Deb, 2020).

5. Performance Experimentation

In this section, we continue our empirical evaluation and validate gains (if any) that arise from the improvements proposed in the previous section. Our setting exactly matches that described in Section 3 in which we consider 108 hyperparameter tuning tasks repeated over 20 random seeds, and utilise normalised score as the evaluation metric.

We also experiment with a wider range of solvers that either rely on BO-strategies or follow zero-order techniques such as differential evolution or particle swarms. These include PySOT a parallel global optimisation package (Eriksson et al., 2019a), OpenTuner a package allowing for ensemble of methods (Ansel et al., 2014), and NeverGrad (Rapin & Teytaud, 2018) a gradient-free optimisation toolbox. Additionally, we carried our modelling improvements to TuRBO, augmenting the standard GP with remedies from Section 4.1 effectively producing a new baseline that we entitle TuRBO+.

Figure 3 demonstrates results showing gains from adopting the general framework, which we designate as G-BO in the plots. In Figure 3 (a), we compare G-BO against other baselines and report up to 8% performance gain compared to a random search strategy. It is also worth noting that TuRBO+ tended to underperform, achieving ca. 4% improvement relative to random search. We believe such a result is related to the interplay between our approach’s capabilities to address heteroscedasticity and non-stationarity as well as the size of the trust-regions; an interesting avenue that we plan to explore in future work. Interestingly, NeverGrad, a model-free solution, also underperformed attaining less

than 2% gain to random search hinting at the importance of a model-based solution. We also elaborate further results in Figure 4 across multiple datasets and models showing that G-BO achieves highest normalised mean scores in 37 out of 54 datasets in total. Further results on all tasks can be found in Appendix A.3.

Ablation Results: Although previous results demonstrate significant advantages of a holistic BO framework, G-BO introduces multiple ingredients affecting performance. To better understand each addition’s contribution, we conducted an ablation study by removing major components and testing those remaining. Specifically, we removed each of the heteroscedastic, non-stationary, robustness, and the multi-acquisition parts, ran BO with the remaining ingredients, and reported average normalised scores and % improvement to random search in Figure 3 (b). First, it is clear that removing any of the components affects performance with some causing about 1% decrease. Second, such a result sheds light on an order of importance between those constituents: Output-Warping \geq Multi-Objective Acquisitions \geq Input-Warping \geq Robustness, where it is understood that \geq reflects performance precedence.

6. Related Work

We introduce work on the following topics relating to modelling, acquisition and optimisers in Bayesian optimisation:

Heteroscedasticity with output transforms: Among various approaches to handling heteroscedasticity (Kersting et al., 2007; Lázaro-Gredilla & Titsias, 2011; Kuindersma et al., 2013; Calandra, 2017; Griffiths et al., 2021), transforming the output variables is a straightforward option giving rise to warped Gaussian processes (Snelson et al., 2004). More recently, output transformations have been extended to compositions of elementary functions (Rios & Tobar, 2019) and normalising flows (Rezende & Mohamed,

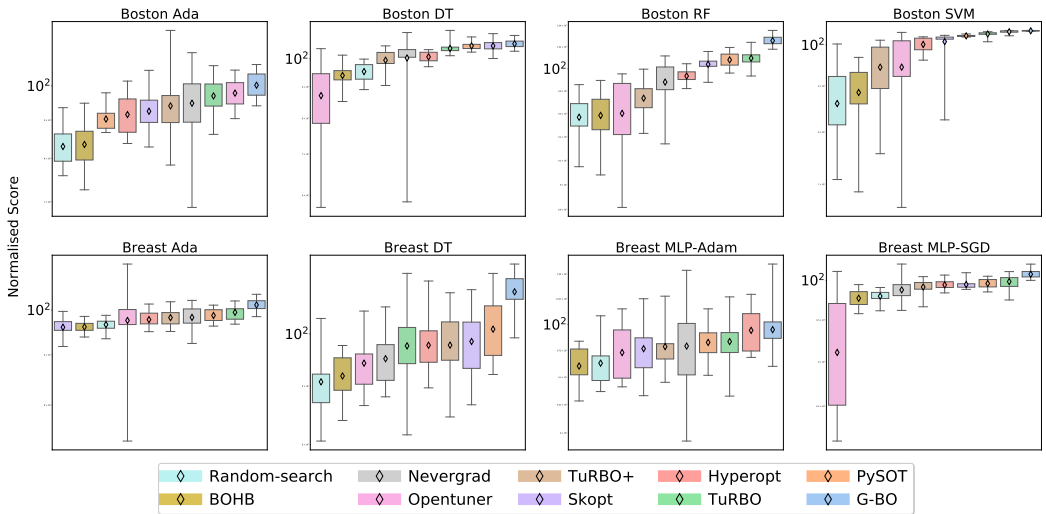


Figure 4. G-BO against all baselines. Each experiment repeated with 20 random seeds. We averaged each seed over both metrics to examine the 54 distinct black-box functions. G-BO achieves the highest normalised mean score in optimising 68.5% of the black-box functions. We highlight 8 of the 54 tasks above, and show the remaining in the Appendix.

2015; Maronas et al., 2020). Output transformations have not featured prominently in the Bayesian optimisation literature, perhaps due to the commonly-held opinion that warped GPs require more data relative to standard GPs in order to function as effective surrogates (Nguyen & Osborne, 2020). Rather than introducing additional hyper-parameters to the GP, we enable efficient output warping through methods that only require pre-training.

Non-stationarity with input warpings: Many surrogate models with input warpings exist for optimising non-stationary black-box objectives (Snoek et al., 2014; Calandra et al., 2016a; Oh et al., 2018) and have enjoyed particular success in hyperparameter tuning where the natural scale of parameters is often logarithmic. Traditionally, a Beta cumulative distribution function is used. In this paper, we adopt the Kumaraswamy warping which is another instance of the generalised Beta class of distributions which we have observed to achieve superior performance to (Snoek et al., 2014); confirming results reported in (Balandat et al., 2020).

Multi-objective acquisition ensembles: Multi-objective acquisition ensembles were first proposed in (Lyu et al., 2018) and are closely related to portfolios of acquisition functions (Hoffman et al., 2011; Shahriari et al., 2014; Balandat et al., 2020). In this form, the optimisation problem involves at least two conflicting and expensive black-box objectives and as such, solutions are located along the Pareto-efficient frontier. The multi-objective acquisition ensemble employs these ideas to find a Pareto-efficient solution amongst multiple acquisition functions. Although we utilised the multi-objective acquisition ensemble, we note that our framework is solver agnostic in so far as any multi-objective optimiser (Abdolshah et al., 2019) may be

applied.

Robustness of Acquisitions: Methods achieving robustness with respect to either surrogates (Park et al., 2020) or the optimisation process (Bogunovic et al., 2018; Bertsimas et al., 2010) have been previously proposed. Most relevant to our setting, is the approach of (Bogunovic et al., 2018) that introduces robustness to BO by solving a max min objective to determine optimal input perturbations. Their method, however, relies on gradient ascent-descent-type algorithms that require real-valued variables and are not guaranteed to converge in the general non-convex, non-concave setting (Lin et al., 2020). On the other hand, our solution possesses two advantages: 1) simplicity of implementation as we merely require random perturbations of acquisition functions to guarantee robustness, and 2) support for mixed variable solutions through the use of evolutionary solvers.

7. Conclusion & Future Work

In this paper, we presented an in-depth empirical study of Bayesian optimisation. We demonstrated that even the simplest among machine learning problems can exhibit heteroscedasticity and non-stationarity. We also reflected on the effects of misspecified models and conflicting acquisition functions. We augmented BO algorithms with various enhancements and revealed that with a revised set of assumptions BO can in fact act as a competitive baseline in hyper-parameter tuning. We hope this paper’s findings can guide the community when employing BO in practice.

In the future, we wish to extend our analysis to high-dimensional domains and consider latent space optimisation (Tripp et al., 2020) in contexts beyond hyper-parameter tun-

ing, including drug discovery, molecule design (Gómez-Bombarelli et al., 2018; Griffiths & Hernández-Lobato, 2020) and robotics (Calandra et al., 2016b).

References

- Abdolshah, M., Shilton, A., Rana, S., Gupta, S., and Venkatesh, S. Multi-objective Bayesian optimisation with preferences over objectives. In *Advances in Neural Information Processing Systems*, volume 32, pp. 12235–12245, 2019.
- Abdullah, M. A., Ren, H., Ammar, H. B., Milenkovic, V., Luo, R., Zhang, M., and Wang, J. Wasserstein robust reinforcement learning. *arXiv preprint arXiv:1907.13196*, 2019.
- Ansel, J., Kamil, S., Veeramachaneni, K., Ragan-Kelley, J., Bosboom, J., O’Reilly, U.-M., and Amarasinghe, S. Opentuner: An extensible framework for program autotuning. In *Proceedings of the 23rd International Conference on Parallel Architectures and Compilation*, pp. 303–316, 2014.
- Balandat, M., Karrer, B., Jiang, D., Daulton, S., Letham, B., Wilson, A. G., and Bakshy, E. BoTorch: A framework for efficient Monte-Carlo Bayesian optimization. *Advances in Neural Information Processing Systems*, 33, 2020.
- Bergstra, J., Komer, B., Eliasmith, C., Yamins, D., and Cox, D. D. Hyperopt: a Python library for model selection and hyperparameter optimization. *Computational Science & Discovery*, 8(1):014008, 2015.
- Bertsimas, D., Nohadani, O., and Teo, K. M. Nonconvex robust optimization for problems with constraints. *INFORMS Journal on Computing*, 22(1):44–58, 2010.
- Blank, J. and Deb, K. Pymoo: Multi-objective optimization in Python. *IEEE Access*, 8:89497–89509, 2020.
- Bobadilla, J., Ortega, F., Hernando, A., and Gutiérrez, A. Recommender systems survey. *Knowledge-Based Systems*, 46:109–132, 2013.
- Bogunovic, I., Scarlett, J., Jegelka, S., and Cevher, V. Adversarially robust optimization with Gaussian processes. In *Proceedings of the 32nd International Conference on Neural Information Processing Systems*, pp. 5765–5775, 2018.
- Box, G. E. and Cox, D. R. An analysis of transformations. *Journal of the Royal Statistical Society: Series B (Methodological)*, 26(2):211–243, 1964.
- Brent, R. P. *Algorithms for minimization without derivatives*. Courier Corporation, 2013.
- Calandra, R. *Bayesian modeling for optimization and control in robotics*. PhD thesis, Darmstadt, Technische Universität, 2017.
- Calandra, R., Peters, J., Rasmussen, C. E., and Deisenroth, M. P. Manifold Gaussian processes for regression. In *2016 International Joint Conference on Neural Networks (IJCNN)*, pp. 3338–3345. IEEE, 2016a.
- Calandra, R., Seyfarth, A., Peters, J., and Deisenroth, M. P. Bayesian optimization for learning gaits under uncertainty. *Annals of Mathematics and Artificial Intelligence*, 76(1):5–23, 2016b.
- Conover, W. J., Johnson, M. E., and Johnson, M. M. A comparative study of tests for homogeneity of variances, with applications to the outer continental shelf bidding data. *Technometrics*, 23(4):351–361, 1981.
- Cowen-Rivers, A. I., Palenicek, D., Moens, V., Abdullah, M., Sootla, A., Wang, J., and Bou-Ammar, H. SAMBA: Safe model-based & active reinforcement learning. *arXiv preprint arXiv:2006.09436*, 2020.
- Deb, K., Pratap, A., Agarwal, S., and Meyerivian, T. A fast and elitist multiobjective genetic algorithm: NSGA-II. *IEEE Transactions on Evolutionary Computation*, 6(2): 182–197, 2002.
- Dua, D. and Graff, C. UCI machine learning repository, 2017. URL <http://archive.ics.uci.edu/ml>.
- Eriksson, D., Bindel, D., and Shoemaker, C. A. pySOT and POAP: An event-driven asynchronous framework for surrogate optimization. *arXiv preprint arXiv:1908.00420*, 2019a.
- Eriksson, D., Pearce, M., Gardner, J., Turner, R. D., and Poloczek, M. Scalable global optimization via local Bayesian optimization. In *Advances in Neural Information Processing Systems*, pp. 5496–5507, 2019b.
- Falkner, S., Klein, A., and Hutter, F. BOHB: Robust and efficient hyperparameter optimization at scale. In *International Conference on Machine Learning*, pp. 1437–1446, 2018.
- Fatima, M. and Pasha, M. Survey of machine learning algorithms for disease diagnostic. *Journal of Intelligent Learning Systems and Applications*, 09:1–16, 2017.
- Fligner, M. A. and Killeen, T. J. Distribution-free two-sample tests for scale. *Journal of the American Statistical Association*, 71(353):210–213, 1976.
- Gabillon, V., Tutunov, R., Valko, M., and Bou-Ammar, H. Derivative-free & order-robust optimisation. In *Proceedings of the Twenty Third International Conference*

- on *Artificial Intelligence and Statistics*, volume 108, pp. 2293–2303, 2020.
- Gómez-Bombarelli, R., Wei, J. N., Duvenaud, D., Hernández-Lobato, J. M., Sánchez-Lengeling, B., Sheberla, D., Aguilera-Iparraguirre, J., Hirzel, T. D., Adams, R. P., and Aspuru-Guzik, A. Automatic chemical design using a data-driven continuous representation of molecules. *ACS central science*, 4(2):268–276, 2018.
- Griffiths, R.-R. and Hernández-Lobato, J. M. Constrained Bayesian optimization for automatic chemical design using variational autoencoders. *Chemical Science*, 11(2): 577–586, 2020.
- Griffiths, R.-R., Aldrick, A. A., Garcia-Ortegon, M., Lalchand, V. R., and Lee, A. A. Achieving robustness to aleatoric uncertainty with heteroscedastic Bayesian optimisation. *arXiv preprint arXiv:1910.07779*, 2021.
- Hansen, N. The CMA evolution strategy: A tutorial. *arXiv preprint arXiv:1604.00772*, 2016.
- Hoffman, M., Brochu, E., and de Freitas, N. Portfolio allocation for Bayesian optimization. In *Proceedings of the Twenty-Seventh Conference on Uncertainty in Artificial Intelligence*, pp. 327–336, 2011.
- Hutter, F., Hoos, H. H., and Leyton-Brown, K. Sequential model-based optimization for general algorithm configuration. In *International Conference on Learning and Intelligent Optimization*, pp. 507–523. Springer, 2011.
- Kandasamy, K., Dasarathy, G., Schneider, J., and Póczos, B. Multi-fidelity Bayesian optimisation with continuous approximations. In *International Conference on Machine Learning*, pp. 1799–1808, 2017.
- Kandasamy, K., Neiswanger, W., Schneider, J., Póczos, B., and Xing, E. P. Neural architecture search with Bayesian optimisation and optimal transport. In *Proceedings of the 32nd International Conference on Neural Information Processing Systems*, pp. 2020–2029, 2018.
- Kersting, K., Plagemann, C., Pfaff, P., and Burgard, W. Most likely heteroscedastic Gaussian process regression. In *Proceedings of the 24th International Conference on Machine Learning*, pp. 393–400, 2007.
- Kingma, D. P. and Ba, J. Adam: A method for stochastic optimization. In Bengio, Y. and LeCun, Y. (eds.), *3rd International Conference on Learning Representations, ICLR 2015, San Diego, CA, USA, May 7-9, 2015, Conference Track Proceedings*, 2015.
- Kingma, D. P. and Welling, M. Auto-encoding variational Bayes. In Bengio, Y. and LeCun, Y. (eds.), *2nd International Conference on Learning Representations, ICLR 2014, Banff, AB, Canada, April 14-16, 2014, Conference Track Proceedings*, 2014.
- Kirschner, J., Bogunovic, I., Jegelka, S., and Krause, A. Distributionally robust Bayesian optimization. In *International Conference on Artificial Intelligence and Statistics*, pp. 2174–2184, 2020.
- Klein, A., Falkner, S., Mansur, N., and Hutter, F. RoBo: A flexible and robust Bayesian optimization framework in Python. In *In Neural Information Processing Systems 2017 Workshop on Bayesian Optimization*, 2017.
- Knudde, N., van der Herten, J., Dhaene, T., and Couckuyt, I. GpflowOpt: a Bayesian optimization library using TensorFlow. In *Neural Information Processing Systems 2017 Workshop on Bayesian Optimization*, 2017.
- Kuindersma, S. R., Grupen, R. A., and Barto, A. G. Variable risk control via stochastic optimization. *The International Journal of Robotics Research*, 32(7):806–825, 2013.
- Kumaraswamy, P. A generalized probability density function for double-bounded random processes. *Journal of Hydrology*, 46(1-2):79–88, 1980.
- Lázaro-Gredilla, M. and Titsias, M. K. Variational heteroscedastic Gaussian process regression. In *Proceedings of the 28th International Conference on International Conference on Machine Learning*, pp. 841–848, 2011.
- Levene, H. Contributions to probability and statistics. *Essays in Honor of Harold Hotelling*, pp. 278–292, 1960.
- Li, L., Jamieson, K., DeSalvo, G., Rostamizadeh, A., and Talwalkar, A. Hyperband: A novel bandit-based approach to hyperparameter optimization. *The Journal of Machine Learning Research*, 18(1):6765–6816, 2017.
- Lin, T., Jin, C., and Jordan, M. On gradient descent ascent for nonconvex-concave minimax problems. In *International Conference on Machine Learning*, pp. 6083–6093, 2020.
- Litjens, G., Kooi, T., Bejnordi, B. E., Setio, A. A. A., Ciompi, F., Ghafoorian, M., Van Der Laak, J. A., Van Ginneken, B., and Sánchez, C. I. A survey on deep learning in medical image analysis. *Medical Image Analysis*, 42: 60–88, 2017.
- Liu, D. C. and Nocedal, J. On the limited memory BFGS method for large scale optimization. *Math. Programming*, 45(3):503–528, 1989.
- Loshchilov, I. and Hutter, F. CMA-ES for hyperparameter optimization of deep neural networks. *arXiv preprint arXiv:1604.07269*, 2016.

- Lyu, W., Yang, F., Yan, C., Zhou, D., and Zeng, X. Batch Bayesian optimization via multi-objective acquisition ensemble for automated analog circuit design. In *International Conference on Machine Learning*, pp. 3306–3314, 2018.
- Maronas, J., Hamelijnck, O., Knoblauch, J., and Damoullas, T. Transforming Gaussian processes with normalizing flows. *arXiv preprint arXiv:2011.01596*, 2020.
- Nguyen, V. and Osborne, M. A. Knowing the what but not the where in Bayesian optimization. In *International Conference on Machine Learning*, pp. 7317–7326, 2020.
- Oh, C., Gavves, E., and Welling, M. Bock: Bayesian optimization with cylindrical kernels. In *International Conference on Machine Learning*, pp. 3868–3877, 2018.
- Park, C. and Lindsay, B. G. Robust scale estimation and hypothesis testing based on quadratic inference function. Technical report, Center for Likelihood Studies, Department of Statistics, The Pennsylvania State University, 1999.
- Park, C., Borth, D. J., Wilson, N. S., Hunter, C. N., and Friedersdorf, F. J. Robust Gaussian process regression with a bias model. *arXiv preprint arXiv:2001.04639*, 2020.
- Pedregosa, F., Varoquaux, G., Gramfort, A., Michel, V., Thirion, B., Grisel, O., Blondel, M., Prettenhofer, P., Weiss, R., Dubourg, V., Vanderplas, J., Passos, A., Cournapeau, D., Brucher, M., Perrot, M., and Duchesnay, E. Scikit-learn: Machine learning in Python. *Journal of Machine Learning Research*, 12:2825–2830, 2011.
- Rapin, J. and Teytaud, O. Nevergrad - A gradient-free optimization platform. <https://GitHub.com/FacebookResearch/Nevergrad>, 2018.
- Rasmussen, C. E. and Williams, C. K. *Gaussian Processes for Machine Learning*, volume 2. MIT press Cambridge, MA, 2006.
- Rezende, D. and Mohamed, S. Variational inference with normalizing flows. In *Proceedings of the 32nd International Conference on Machine Learning*, volume 37, pp. 1530–1538, 2015.
- Rios, G. and Tobar, F. Compositionally-warped Gaussian processes. *Neural Networks*, 118:235–246, 2019.
- Sen, R., Kandasamy, K., and Shakkottai, S. Multi-fidelity black-box optimization with hierarchical partitions. In *International Conference on Machine Learning*, pp. 4538–4547. PMLR, 2018.
- Shahriari, B., Wang, Z., Hoffman, M. W., Bouchard-Côté, A., and de Freitas, N. An entropy search portfolio for Bayesian optimization. *arXiv preprint arXiv:1406.4625*, 2014.
- Snelson, E., Rasmussen, C. E., and Ghahramani, Z. Warped Gaussian processes. *Advances in Neural Information Processing Systems*, 16:337–344, 2004.
- Snoek, J., Larochelle, H., and Adams, R. P. Practical Bayesian optimization of machine learning algorithms. In *Advances in Neural Information Processing Systems*, pp. 2951–2959, 2012.
- Snoek, J., Swersky, K., Zemel, R., and Adams, R. Input warping for Bayesian optimization of non-stationary functions. In *International Conference on Machine Learning*, pp. 1674–1682, 2014.
- Springenberg, J. T., Klein, A., Falkner, S., and Hutter, F. Bayesian optimization with robust Bayesian neural networks. In *Advances in Neural Information Processing Systems*, pp. 4134–4142, 2016.
- Tobin, J., Fong, R., Ray, A., Schneider, J., Zaremba, W., and Abbeel, P. Domain randomization for transferring deep neural networks from simulation to the real world. In *2017 IEEE/RSJ International Conference on Intelligent Robots and Systems (IROS)*, pp. 23–30. IEEE, 2017.
- Tripp, A., Daxberger, E., and Hernández-Lobato, J. M. Sample-efficient optimization in the latent space of deep generative models via weighted retraining. *Advances in Neural Information Processing Systems*, 33, 2020.
- Wilson, A. C., Roelofs, R., Stern, M., Srebro, N., and Recht, B. The marginal value of adaptive gradient methods in machine learning. In *Proceedings of the 31st International Conference on Neural Information Processing Systems*, pp. 4151–4161, 2017.
- Yeo, I.-K. and Johnson, R. A. A new family of power transformations to improve normality or symmetry. *Biometrika*, 87(4):954–959, 2000.

A. Experimental Details

A.1. Black-Box Functions

As specified in Section 3, we evaluate black-box optimisation solvers based on their performances on a large set of tasks from `Bayesmark` package. Each task consists in optimising the hyperparameters of a model to minimise the cross validation loss incurred when this model is applied to perform a regression (reg) or a classification (clf) on a given dataset. Thus, a task is characterised by a model, a dataset and a loss function, or metric, measuring the quality of the regression or classification. In total, 108 distinct tasks can be defined from the valid combination of the nine models specified in Table 1, the following six real-world UCI datasets (Dua & Graff, 2017), Boston (reg), Breast Cancer (clf), Diabetes (reg), Digits (clf), Iris (clf) and Wine (clf); the following two regression metrics, negative mean-squared error (MSE), negative mean absolute error (MAE), and two classification metrics, negative log-likelihood (NLL) and negative accuracy (ACC). The results reported on Figures 3 and 4 have been obtained by applying each black-box optimisation method using 16 iterations of 8-batch acquisition steps on all of the 108 tasks. In order to provide a reliable evaluation of the different solvers, we repeated each run with 20 random seeds and considered the normalised score given by:

$$\text{Normalised Score} = 100 \times \frac{\mathcal{L} - \mathcal{L}^*}{\mathcal{L}^{\text{rand}} - \mathcal{L}^*} \quad (3)$$

where \mathcal{L} is the best-achieved cross validation loss at the end of the 16 acquisition steps, \mathcal{L}^* is the estimated optimal loss for the task and $\mathcal{L}^{\text{rand}}$ is the mean loss (across multiple runs) obtained using random search with the same number of acquisition steps. The normalisation procedure allows to aggregate the scores across tasks although different cross-validation loss functions were used.

A.2. Black-Box Optimisation Variables

We provide in Table 1 and Table 2 the list of the hyperparameters controlling the behaviour of each model along with their optimisation domains, which can differ whether the model is used for a classification or a regression task. The search domain can include a mix of continuous and integer variables (e.g. MLP-SGD set of hyperparameters includes a hidden layer size, which needs to be an integer, and an initial learning rate that can take any values between 10^{-5} and 10^{-1}), and its dimensionality - which corresponds to the number of hyperparameters to tune - ranges from 2 to 9. We also specify in the last column of these Tables whether the search domain is modified through a standard transformation (log or logit) to ease optimisation.

A.3. Additional results

Table 3 synthesises the performances achieved on the 108 tasks by the black-box optimisation solvers considered in our experiments. We note that the distribution of the scores attained by `G-BO` has the largest mean and the smallest standard-deviation, indicating significant out-performance of this method over alternative solvers. In complement, normalised score distributions obtained on each task by each black-box optimisers are provided on Figure 5.

A.4. Implementation details on BOHB

BOHB is a scalable hyper-parameter tuning algorithm introduced in (Falkner et al., 2018) mixing bandits and BO approaches to achieve strong anytime and final performances. Contrary to the other solvers considered in this paper, BOHB is specifically designed to tackle multi-fidelity optimisation and it uses Hyperband (Li et al., 2017) routine to define the fidelity levels under which points are asynchronously evaluated. The selection of points follows a BO strategy based on Tree Parzen Estimator (TPE) method. Given a set \mathcal{D} of already observed data points and a threshold $\alpha \in \mathbb{R}$, the TPE models $p(\mathbf{x}|y)$ using kernel density estimations of

$$\begin{aligned} \ell(\mathbf{x}) &= p(y < \alpha | \mathbf{x}, \mathcal{D}) \\ g(\mathbf{x}) &= p(y \geq \alpha | \mathbf{x}, \mathcal{D}). \end{aligned}$$

In the TPE algorithm, maximising the expected improvement criterion

$$\alpha_{\text{EI}}(\mathbf{x}) = \int \max(0, \alpha - p(y|\mathbf{x}))p(y|\mathbf{x})dy$$

is equivalent to maximising the ratio $r(\mathbf{x}) = \frac{\ell(\mathbf{x})}{g(\mathbf{x})}$ which is carried out to select a single new candidate point at a time.

In the absence of a multi-fidelity setup in our experiments, we ran a modified version of the BOHB algorithm implemented in `HpBandSter` package. We left TPE method for modelling unchanged, but we ignored fidelity level assignment from Hyperband. Moreover, as our experimental setup involves batch-acquisitions, we tested two alternatives to standard BOHB acquisition procedure to support synchronous suggestion of multiple points. In a first approach, we run q independent maximisation processes of $r(\mathbf{x})$ from random starting points and recover a single candidate from each process to form the q -batch suggestion. In a second approach, we obtain one point as a result of a single maximisation of $r(\mathbf{x})$ and we sample $q - 1$ random points to complete the q -batch suggestion. As the latter method yields better overall performance, the results reported in this work under BOHB label have been obtained using the second approach.

Table 1. Search spaces for hyperparameter tuning on classification tasks. We specify the type of each hyperparameters (with \mathbb{R} for real-valued and \mathbb{Z} for integer valued) as well as the search domain. We specify $\log -\mathcal{U}$ (resp. $\text{logit} - \mathcal{U}$) to indicate that a log (resp. logit) transformation is applied to the optimisation domain.

Model	Parameter	Type	Domain
kNN	n_neighbors	\mathbb{Z}	$\mathcal{U}(1, 25)$
	p	\mathbb{Z}	$\mathcal{U}(1, 4)$
Support Vector Machine	C	\mathbb{R}	$\log -\mathcal{U}(1, 10^3)$
	gamma	\mathbb{R}	$\log -\mathcal{U}(10^{-4}, 10^{-3})$
	tol	\mathbb{R}	$\log -\mathcal{U}(10^{-5}, 10^{-1})$
	max_depth	\mathbb{Z}	$\mathcal{U}(1, 15)$
Decision Tree	min_samples_split	\mathbb{R}	$\text{logit} - \mathcal{U}(0.01, 0.99)$
	min_samples_leaf	\mathbb{R}	$\text{logit} - \mathcal{U}(0.01, 0.49)$
	min_weight_fraction_leaf	\mathbb{R}	$\text{logit} - \mathcal{U}(0.01, 0.49)$
	max_features	\mathbb{R}	$\text{logit} - \mathcal{U}(0.01, 0.99)$
	min_impurity_decrease	\mathbb{R}	$\mathcal{U}(0, 0.5)$
Random Forest	max_depth	\mathbb{Z}	$\mathcal{U}(1, 15)$
	max_features	\mathbb{R}	$\text{logit} - \mathcal{U}(0.01, 0.99)$
	min_samples_split	\mathbb{R}	$\text{logit} - \mathcal{U}(0.01, 0.99)$
	min_samples_leaf	\mathbb{R}	$\text{logit} - \mathcal{U}(0.01, 0.49)$
	min_weight_fraction_leaf	\mathbb{R}	$\text{logit} - \mathcal{U}(0.01, 0.49)$
	min_impurity_decrease	\mathbb{R}	$\mathcal{U}(0, 0.5)$
MLP-Adam	hidden_layer_sizes	\mathbb{Z}	$\mathcal{U}(50, 200)$
	alpha	\mathbb{R}	$\log -\mathcal{U}(10^{-5}, 10^1)$
	batch_size	\mathbb{Z}	$\mathcal{U}(10, 250)$
	learning_rate_init	\mathbb{R}	$\log -\mathcal{U}(10^{-5}, 10^{-1})$
	tol	\mathbb{R}	$\log -\mathcal{U}(10^{-5}, 10^{-1})$
	validation_fraction	\mathbb{R}	$\text{logit} - \mathcal{U}(0.1, 0.9)$
	beta_1	\mathbb{R}	$\text{logit} - \mathcal{U}(0.5, 0.99)$
	beta_2	\mathbb{R}	$\text{logit} - \mathcal{U}(0.9, 1 - 10^{-6})$
	epsilon	\mathbb{R}	$\log -\mathcal{U}(10^{-9}, 10^{-6})$
	hidden_layer_sizes	\mathbb{Z}	$\mathcal{U}(50, 200)$
MLP-SGD	alpha	\mathbb{R}	$\log -\mathcal{U}(10^{-5}, 10^1)$
	batch_size	\mathbb{Z}	$\mathcal{U}(10, 250)$
	learning_rate_init	\mathbb{R}	$\log -\mathcal{U}(10^{-5}, 10^{-1})$
	power_t	\mathbb{R}	$\text{logit} - \mathcal{U}(0.1, 0.9)$
	tol	\mathbb{R}	$\log -\mathcal{U}(10^{-5}, 10^{-1})$
	momentum	\mathbb{R}	$\text{logit} - \mathcal{U}(0.001, 0.999)$
	validation_fraction	\mathbb{R}	$\text{logit} - \mathcal{U}(0.1, 0.9)$
	n_estimators	\mathbb{Z}	$\mathcal{U}(10, 100)$
AdaBoost	learning_rate	\mathbb{R}	$\log -\mathcal{U}(10^{-4}, 10^1)$
	learning_rate	\mathbb{R}	$\log -\mathcal{U}(10^{-2}, 10^2)$
Lasso	intercept_scaling	\mathbb{R}	$\log -\mathcal{U}(10^{-2}, 10^2)$
	intercept_scaling	\mathbb{R}	$\log -\mathcal{U}(10^{-2}, 10^2)$
Linear	C	\mathbb{R}	$\log -\mathcal{U}(10^{-2}, 10^2)$
	intercept_scaling	\mathbb{R}	$\log -\mathcal{U}(10^{-2}, 10^2)$

Generalised Bayesian Optimisation

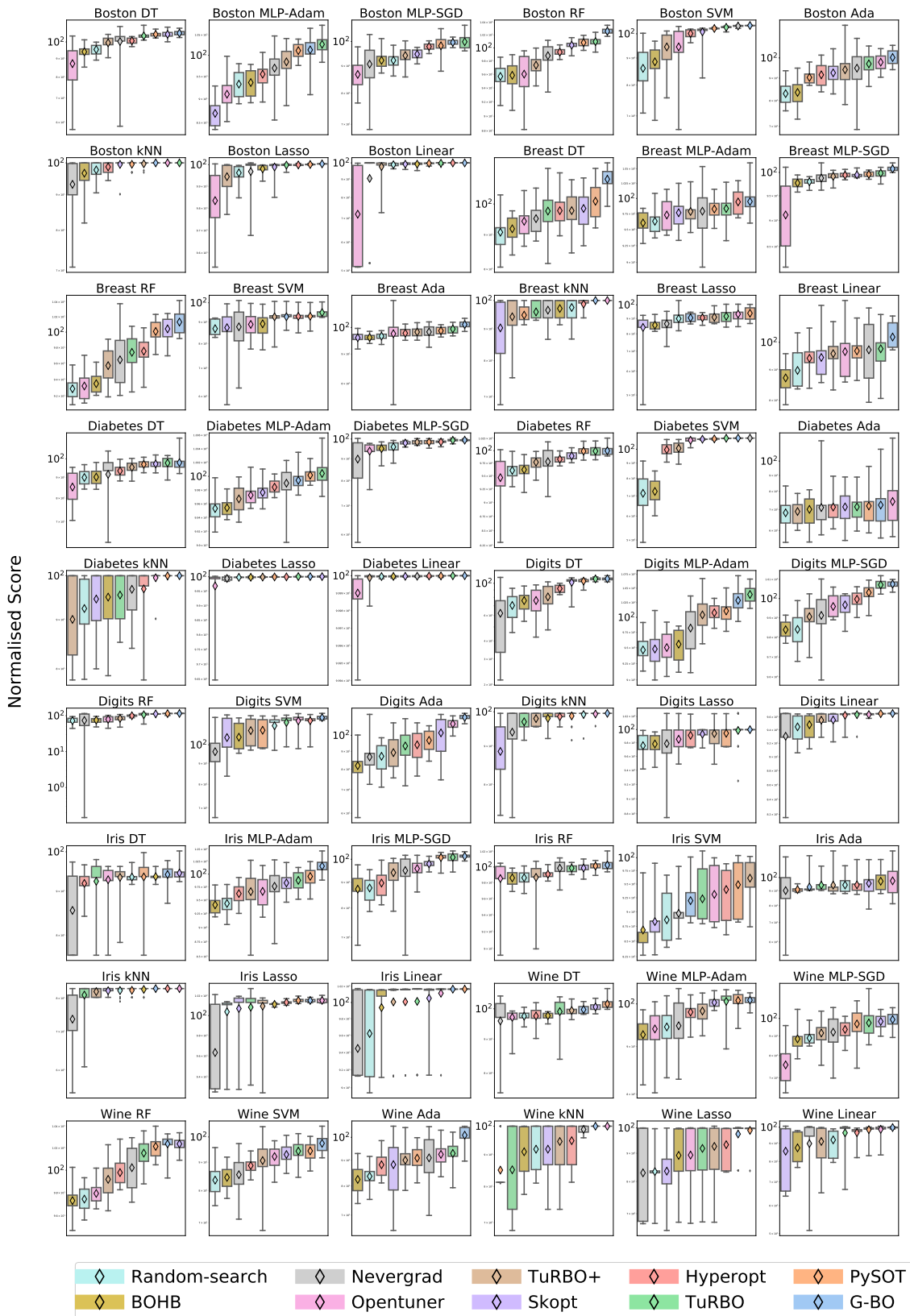


Figure 5. Normalised score (see 3) obtained by each black-box optimiser on all tasks. On each graph optimisers are ranked by mean scores.

Table 2. Models and search spaces for hyperparameter tuning on regression tasks. Models having same search spaces for classification and regression tasks are omitted (see Table 1).

Model	Parameter	Type	Domain
AdaBoost	n_estimators	\mathbb{Z}	$\mathcal{U}(10, 100)$
	learning_rate	\mathbb{R}	$\log -\mathcal{U}(10^{-4}, 10^1)$
Lasso	alpha	\mathbb{R}	$\log -\mathcal{U}(10^{-2}, 10^2)$
	fit_intercept	\mathbb{Z}	$\mathcal{U}(0, 1)$
	normalize	\mathbb{Z}	$\mathcal{U}(0, 1)$
	max_iter	\mathbb{Z}	$\log -\mathcal{U}(10, 5000)$
	tol	\mathbb{R}	$\log -\mathcal{U}(10^{-5}, 10^{-1})$
	positive	\mathbb{Z}	$\mathcal{U}(0, 1)$
Linear	alpha	\mathbb{R}	$\log -\mathcal{U}(10^{-2}, 10^2)$
	fit_intercept	\mathbb{Z}	$\mathcal{U}(0, 1)$
	normalize	\mathbb{Z}	$\mathcal{U}(0, 1)$
	max_iter	\mathbb{Z}	$\log -\mathcal{U}(10, 5000)$
	tol	\mathbb{R}	$\log -\mathcal{U}(10^{-4}, 10^{-1})$

Algorithm	Mean	Std	Median	40 th Centile	30 th Centile	20 th Centile	5 th Centile
G-BO	100.12	8.70	100.01	100.00	99.88	98.64	85.71
PySot	98.18	9.03	100.00	99.81	98.60	95.36	80.00
TuRBO	97.95	10.80	100.00	99.88	98.75	95.26	78.63
HyperOpt	96.37	8.79	99.31	98.16	95.94	92.38	78.52
SkOpt	96.18	11.51	99.78	98.66	96.73	91.62	74.77
TuRBO+	95.29	10.93	98.97	97.60	95.27	90.92	74.77
OpenTuner	94.32	14.18	98.44	96.93	93.84	89.97	68.96
NeverGrad	93.20	17.52	99.65	97.84	94.57	88.28	55.34
BOHB	92.03	11.16	96.02	93.55	90.14	85.71	67.82
Random-Search	92.00	11.71	96.18	93.55	90.05	85.16	69.55

Table 3. Mean and n-th percentile normalized scores over 108 black-box functions, each repeated with 20 random seeds. We see significant mean improvements from G-BO compared with all other algorithms.

B. Heteroschedasticity Testing

GP modelling usually considers a conditional normal distribution of the observations $y_i | \cdot \sim \mathcal{N}(f(\cdot), \sigma^2(\cdot))$. In most cases GP regression is run assuming $\sigma(\cdot)^2$ to be constant, in which case the GP is called homoscedastic. To assess whether this assumption holds for the tasks under examination, we used Levine’s test and Fligner and Killeen test.

To run these tests on a given task, we evaluated $k = 50$ distinct sets of hyperparameters $\{x_i\}_{1 \leq i \leq k}$ for $n = 10$ times and obtained scores $\{Y_{ij}\}_{1 \leq i \leq k, 1 \leq j \leq n}$, where Y_{ij} is the j^{th} score observed when evaluating the i^{th} configuration. For $i = 1, \dots, k$, let σ_i^2 denote the observed variance of $y|x_i$, then both Levine’s and Fligner and Killeen tests share the same null hypothesis of homoscedasticity:

$$H_0 : \sigma_1^2 = \dots = \sigma_k^2.$$

B.1. Levine’s test

Levine’s test statistic is defined as

$$W = \frac{N - k}{k - 1} \cdot \frac{\sum_{i=1}^k n(\bar{Z}_i - \bar{Z}_{..})^2}{\sum_{i=1}^k \sum_{j=1}^n (Z_{ij} - \bar{Z}_i)^2}$$

where $N = k \times n$, $Z_{ij} = |Y_{ij} - \frac{1}{n} \sum_{j=1}^n Y_{ij}|$, $\bar{Z}_i = \frac{1}{n} \sum_{j=1}^n Z_{ij}$ and $\bar{Z}_{..} = \frac{1}{k} \sum_{i=1}^k \bar{Z}_i$, for all $i = 1, \dots, k$, $j = 1, \dots, n$. The Levine test rejects homoscedasticity hypothesis H_0 if

$$W > F_{\alpha, k-1, N-k}$$

where $F_{\alpha, k-1, N-k}$ is the upper critical value at a significance level α of the F distribution with $k - 1$ and $N - k$ degrees of freedom.

Fligner and Killen test is an alternative to Levine’s test that is particularly robust to outliers.

B.2. Fligner & Killen test

Computation of Fligner and Killen test requires ranking all the absolute values $\{|Y_{ij} - \tilde{Y}_i|\}_{1 \leq i \leq k, 1 \leq j \leq n}$ where Y_i is the median of $\{Y_{ij}\}_{1 \leq j \leq n}$. Increasing scores $a_{N,r} = \Phi^{-1}\left(\frac{1+\frac{r}{N+1}}{2}\right)$ are associated to each rank $r = 1, \dots, N$, where $N = kn$ and $\Phi(\cdot)$ is the cumulative distribution function for standard Normal variable. We denote the rank score associated to Y_{ij} as r_{ij} .

The Fligner and Killen test statistic is given by

$$\chi_0^2 = \frac{\sum_{i=1}^k n (\bar{A}_i - \bar{a})^2}{V^2}$$

where $\bar{A}_i = \frac{1}{n} \sum_{j=1}^n a_{N,r_{ij}}$, $\bar{a} = \frac{1}{N} \sum_{r=1}^N a_{N,r}$ and $V^2 = \frac{1}{N-1} \sum_{r=1}^N (a_{N,r} - \bar{a})^2$.

As χ_0 has asymptotic χ^2 distribution with $(k-1)$ degrees of freedom, therefore the test rejects homoscedasticity hypothesis H_0 if

$$\chi_0 > \chi_{\alpha, k-1}^2$$

where $\chi_{\alpha, k-1}^2$ is the upper critical value at a significance level α of the χ^2 distribution with $k-1$ degrees of freedom.

The results of Levine test as well as Fligner and Killen test are reported on Table 10-15.

C. Further Mathematical Details

C.1. GP posterior

Under a GP assumption with Gaussian-corrupted observations $y_\ell = f(\mathbf{x}_\ell) + \epsilon_\ell$ where $\epsilon_\ell \sim \mathcal{N}(0, \sigma^2)$, and given a set $\mathcal{D} = \{\mathbf{x}, \mathbf{y}\}$ of available data, the joint distribution of \mathcal{D} and an arbitrary set of input points $\mathbf{x}_{1:q}$ is given by

$$\begin{aligned} & \left[\begin{array}{c} \mathbf{y} \\ f(\mathbf{x}_{1:q}) \end{array} \right] \Big| \boldsymbol{\theta} \sim \\ & \mathcal{N} \left(\left[\begin{array}{cc} m(\mathbf{x}) & \mathbf{K}_\theta + \sigma^2 \mathbf{I} \\ m(\mathbf{x}_{1:q}) & \mathbf{k}_\theta^\top(\mathbf{x}_{1:q}) \end{array} \right], \left[\begin{array}{cc} \mathbf{K}_\theta + \sigma^2 \mathbf{I} & \mathbf{k}_\theta(\mathbf{x}_{1:q}) \\ \mathbf{k}_\theta^\top(\mathbf{x}_{1:q}) & \mathbf{k}_\theta(\mathbf{x}_{1:q}, \mathbf{x}_{1:q}) \end{array} \right] \right), \end{aligned}$$

where $\mathbf{K}_\theta = \mathbf{K}_\theta(\mathbf{x}, \mathbf{x})$ and $\mathbf{k}_\theta(\mathbf{x}_{1:q}) = \mathbf{k}_\theta(\mathbf{x}, \mathbf{x}_{1:q})$. From this joint distribution one can derive though marginalisation (Rasmussen & Williams, 2006) the predictive posterior $p(f(\mathbf{x}_{1:q})|\mathcal{D}) = \mathcal{N}(\boldsymbol{\mu}_\theta(\mathbf{x}_{1:q}), \boldsymbol{\Sigma}_\theta(\mathbf{x}_{1:q}))$ with:

$$\begin{aligned} \boldsymbol{\mu}_\theta(\mathbf{x}_{1:q}) &= m(\mathbf{x}_{1:q}) \\ &+ \mathbf{k}_\theta(\mathbf{x}_{1:q})^\top (\mathbf{K}_\theta + \sigma^2 \mathbf{I})^{-1} (\mathbf{y} - m(\mathbf{x})) \\ \boldsymbol{\Sigma}_\theta(\mathbf{x}_{1:q}) &= \mathbf{K}_\theta(\mathbf{x}_{1:q}, \mathbf{x}_{1:q}) \\ &- \mathbf{k}_\theta(\mathbf{x}_{1:q})^\top (\mathbf{K}_\theta + \sigma^2 \mathbf{I})^{-1} \mathbf{k}_\theta(\mathbf{x}_{1:q}) \end{aligned}$$

C.2. Yeo-Johnson Transform

When labels take on arbitrary values, we use a Yeo-Johnson transform instead of Box-Cox. Such a

transformation operates as follows:

$$Y \cdot J \cdot \zeta(y_l) = \begin{cases} \frac{(y_l+1)^\zeta - 1}{\zeta}, & \text{if } \zeta \neq 0, y_l \geq 0 \\ \log(y_l + 1), & \text{if } \zeta = 0, y_l \geq 0 \\ \frac{(1-y_l)^{2-\zeta} - 1}{\zeta-2}, & \text{if } \zeta \neq 2, y_l < 0 \\ -\log(1 - y_l) & \text{if } \zeta = 2, y_l < 0. \end{cases}$$

Analogous to the Box-Cox transform, the Yeo-Johnson's parameter is fit based on observed data solving the following 1-dimensional optimisation problem:

$$\begin{aligned} \max_{\zeta} -\frac{n}{2} \log \left[\frac{\sum_{j=1}^n (Y \cdot J \cdot \zeta(y_l) - \overline{Y \cdot J \cdot \zeta(\mathbf{y})})^2}{n-1} \right] \\ + (\zeta - 1) \sum_{i=1}^n [\text{sign}(y_l) \log(|y_l| + 1)], \end{aligned}$$

with $\overline{Y \cdot J \cdot \zeta(\mathbf{y})}$ being the sample average computed after applying the Yeo-Johnson transformation.

C.3. Robust Acquisition Objectives

Notice, the robust form of acquisition function given as $\alpha_{\text{rob}}(\mathbf{x}|\mathcal{D}) \equiv \mathbb{E}_{\epsilon \sim \mathcal{N}(\mathbf{0}, \sigma_\epsilon^2 \mathbf{I})} [\alpha^{\theta+\epsilon}(\mathbf{x}|\mathcal{D})]$ constitutes an intractable integral. Therefore, in order to be maximised during BO execution, it should be replaced with accurate approximation. Our next result establishes such arbitrary accurate approximation with high probability.

Lemma: Let $\delta \in (0, 1)$ be a desirable probability threshold, and $\rho \in (0, 1)$ be a desirable accuracy parameter. Consider the GP process with mean function $m(\mathbf{x})$ and covariance function $k_\theta(\mathbf{x}, \mathbf{x}')$ such that $\forall \mathbf{x}, \mathbf{x}' \in \mathcal{X}, \boldsymbol{\theta} \in \mathbb{R}^p$:

$$\begin{aligned} |k_\theta(\mathbf{x}, \mathbf{x})| &\geq M_0, \quad |k_\theta(\mathbf{x}, \mathbf{x}')| \leq M_1, \\ \|\nabla_{\boldsymbol{\theta}} k_\theta(\mathbf{x}, \mathbf{x}')\|_2 &\leq M_2, \quad |m(\mathbf{x})| \leq M_4. \end{aligned} \quad (4)$$

Moreover, assume that observations $y \in \mathcal{D}$ are bounded, i.e. $|y| \leq C$ and let $\bar{\alpha}^\theta(\mathbf{x}|\mathcal{D}) = \alpha^\theta(\mathbf{x}|\mathcal{D}) + \eta \sigma_n$ with η being standard normal random variable. Then, there are constants c_1 and c_2 , such that choosing $\sigma_n \leq c_1$ and $\sigma_\epsilon \leq c_2$:

$$|\bar{\alpha}^\theta(\mathbf{x}|\mathcal{D}) - \mathbb{E}_{\epsilon \sim \mathcal{N}(\mathbf{0}, \sigma_\epsilon^2 \mathbf{I})} [\alpha^{\theta+\epsilon}(\mathbf{x}|\mathcal{D})]| \leq \rho.$$

with probability at least $1 - \delta$.

Proof. Without loss of generality we chose UCB acquisition function $\alpha(\mathbf{x})^\theta(\mathbf{x}|\mathcal{D}) = \alpha_{\text{UCB}}(\mathbf{x})^\theta(\mathbf{x}|\mathcal{D})$ and to avoid technical complications related to multivariate calculus we consider batch size $q = 1$. In this case, UCB acquisition function can be written as $\alpha_{\text{UCB}}(\mathbf{x})^\theta(\mathbf{x}|\mathcal{D}) = \mu_\theta(\mathbf{x}|\mathcal{D}) + \sqrt{\frac{\beta\pi}{2}} \sigma_\theta(\mathbf{x}|\mathcal{D})$, where $\mu_\theta(\mathbf{x}|\mathcal{D})$ and $\sigma_\theta(\mathbf{x}|\mathcal{D})$ are posterior mean and posterior deviation respectively.

Consider an Monte-Carlo estimation of $\alpha_{\text{rob.}}(\mathbf{x}|\mathcal{D}) \equiv \mathbb{E}_{\epsilon \sim \mathcal{N}(\mathbf{0}, \sigma_\epsilon^2 \mathbf{I})} [\alpha^{\theta+\epsilon}(\mathbf{x}|\mathcal{D})]$:

$$\hat{\alpha}^\theta(\mathbf{x}|\mathcal{D}) = \frac{1}{N_\epsilon} \sum_{j=1}^{N_\epsilon} \alpha^{\theta+\epsilon_j}(\mathbf{x}|\mathcal{D})$$

where ϵ_j are i.i.d. samples drawn from $\mathcal{N}(\mathbf{0}, \sigma_\epsilon^2 \mathbf{I})$. Then, adding and subtracting $\hat{\alpha}^\theta(\mathbf{x}|\mathcal{D})$ gives:

$$\begin{aligned} & |\bar{\alpha}^\theta(\mathbf{x}|\mathcal{D}) - \mathbb{E}_{\epsilon \sim \mathcal{N}(\mathbf{0}, \sigma_\epsilon^2 \mathbf{I})} [\alpha^{\theta+\epsilon}(\mathbf{x}|\mathcal{D})]| \leq \\ & |\bar{\alpha}^\theta(\mathbf{x}|\mathcal{D}) - \hat{\alpha}^\theta(\mathbf{x}|\mathcal{D})| + \\ & |\hat{\alpha}^\theta(\mathbf{x}|\mathcal{D}) - \mathbb{E}_{\epsilon \sim \mathcal{N}(\mathbf{0}, \sigma_\epsilon^2 \mathbf{I})} [\alpha^{\theta+\epsilon}(\mathbf{x}|\mathcal{D})]|. \end{aligned}$$

Using definition of $\hat{\alpha}^\theta(\mathbf{x}|\mathcal{D})$ in the above result gives:

$$\begin{aligned} & |\bar{\alpha}^\theta(\mathbf{x}|\mathcal{D}) - \mathbb{E}_{\epsilon \sim \mathcal{N}(\mathbf{0}, \sigma_\epsilon^2 \mathbf{I})} [\alpha^{\theta+\epsilon}(\mathbf{x}|\mathcal{D})]| \leq \quad (5) \\ & \frac{1}{N_\epsilon} \sum_{j=1}^{N_\epsilon} |\bar{\alpha}^\theta(\mathbf{x}|\mathcal{D}) - \alpha^{\theta+\epsilon_j}(\mathbf{x}|\mathcal{D})| + \\ & \left| \frac{1}{N_\epsilon} \sum_{j=1}^{N_\epsilon} \alpha^{\theta+\epsilon_j}(\mathbf{x}|\mathcal{D}) - \mathbb{E}_{\epsilon \sim \mathcal{N}(\mathbf{0}, \sigma_\epsilon^2 \mathbf{I})} [\alpha^{\theta+\epsilon}(\mathbf{x}|\mathcal{D})] \right| \end{aligned}$$

Let us study separately each term in the above result. Applying Chebyshev inequality for the second term in the above expression, we have that with probability at least $p_1 = 1 - \frac{8[\mathbb{E}_\epsilon [\mu_{\theta+\epsilon}^2(\mathbf{x}|\mathcal{D})] + \frac{\beta\pi}{2} \mathbb{E}_\epsilon [\sigma_{\theta+\epsilon}^2(\mathbf{x}|\mathcal{D})]]}{N_\epsilon \rho^2}$:

$$\left| \frac{1}{N_\epsilon} \sum_{j=1}^{N_\epsilon} \alpha^{\theta+\epsilon_j}(\mathbf{x}|\mathcal{D}) - \mathbb{E}_{\epsilon \sim \mathcal{N}(\mathbf{0}, \sigma_\epsilon^2 \mathbf{I})} [\alpha^{\theta+\epsilon}(\mathbf{x}|\mathcal{D})] \right| \leq \frac{\rho}{2}. \quad (6)$$

In order to ensure that $p_1 = 1 - \frac{\delta}{2}$ the number of samples ϵ_j should be taken:

$$N_\epsilon = \left\lceil \frac{16 \left[\mathbb{E}_\epsilon [\mu_{\theta+\epsilon}^2(\mathbf{x}|\mathcal{D})] + \frac{\beta\pi}{2} \mathbb{E}_\epsilon [\sigma_{\theta+\epsilon}^2(\mathbf{x}|\mathcal{D})] \right]}{\delta \rho^2} \right\rceil.$$

We will simplify this expression using bounds in 4 later. Now, let us focus on the second term in Inequality 5. To bound it, we are going to establish a bound on $|\bar{\alpha}^\theta(\mathbf{x}|\mathcal{D}) - \alpha^{\theta+\epsilon_j}(\mathbf{x}|\mathcal{D})|$. For small random perturbation ϵ_j we have (with probability 1):

$$\begin{aligned} \alpha^{\theta+\epsilon_j}(\mathbf{x}|\mathcal{D}) &= \alpha^\theta(\mathbf{x}|\mathcal{D}) + \epsilon_j^\top \nabla_\theta \alpha^\theta(\mathbf{x}|\mathcal{D}) + o(\|\epsilon_j\|) = \\ \alpha^\theta(\mathbf{x}|\mathcal{D}) &+ \epsilon_j^\top \nabla_\theta \left[\mu_\theta(\mathbf{x}|\mathcal{D}) + \sqrt{\frac{\beta\pi}{2}} \sigma_\theta(\mathbf{x}|\mathcal{D}) \right] \\ &+ o(\|\epsilon_j\|_2). \end{aligned}$$

Let us denote

$$\mathbf{h}_\theta(\mathbf{x}|\mathcal{D}) = \nabla_\theta \left[\mu_\theta(\mathbf{x}|\mathcal{D}) + \sqrt{\frac{\beta\pi}{2}} \sigma_\theta(\mathbf{x}|\mathcal{D}) \right]$$

then, using Cauchy–Schwarz inequality we have:

$$|\alpha^{\theta+\epsilon_j}(\mathbf{x}|\mathcal{D}) - \alpha^\theta(\mathbf{x}|\mathcal{D})| \leq \|\epsilon_j\|_2 \|\mathbf{h}_\theta(\mathbf{x}|\mathcal{D})\|_2 + o(1)$$

Since $\epsilon_j \sim \mathcal{N}(0, 1)$, then with probability at least $1 - \frac{\delta}{4N_\epsilon}$:

$$\|\epsilon_j\|_2 \leq 4\sigma_\epsilon \sqrt{p} + 2\sigma_\epsilon \sqrt{\log \frac{4N_\epsilon}{\delta}}$$

Let us assume (and later we will prove the existence of such bound) that $\|\mathbf{h}_\theta(\mathbf{x}|\mathcal{D})\|_2 \leq A_1$. Then, with probability at least $1 - \frac{\delta}{4N_\epsilon}$:

$$\begin{aligned} & |\alpha^{\theta+\epsilon_j}(\mathbf{x}|\mathcal{D}) - \alpha^\theta(\mathbf{x}|\mathcal{D})| \leq \\ & \left[4\sigma_\epsilon \sqrt{p} + 2\sigma_\epsilon \sqrt{\log \frac{4N_\epsilon}{\delta}} \right] [A_1 + o(1)] \end{aligned}$$

On the other hand, for $\bar{\alpha}^\theta(\mathbf{x}|\mathcal{D}) = \alpha^\theta(\mathbf{x}|\mathcal{D}) + \eta\sigma_\eta$ with probability at least $1 - \frac{\delta}{4N_\epsilon}$ we have:

$$|\bar{\alpha}^\theta(\mathbf{x}|\mathcal{D}) - \alpha^\theta(\mathbf{x}|\mathcal{D})| \leq \Phi^{-1} \left(1 - \frac{\delta}{8N_\epsilon} \right) \sigma_n.$$

where $\Phi(\cdot)$ is cumulative distribution function for standard Gaussian variable. Hence, by choosing $\sigma_\epsilon = \min \left\{ 1, \frac{\Phi^{-1} \left(1 - \frac{\delta}{8N_\epsilon} \right) \sigma_n}{\left[4\sqrt{p} + 2\sqrt{\log \frac{4N_\epsilon}{\delta}} \right] [A_1 + o(1)]} \right\}$ with probability at least $1 - \frac{\delta}{2N_\epsilon}$ we have that both $\bar{\alpha}^\theta(\mathbf{x}|\mathcal{D})$ and $\alpha^{\theta+\epsilon_j}(\mathbf{x}|\mathcal{D})$ belong to the interval centred at $\alpha^\theta(\mathbf{x}|\mathcal{D})$ of size $\Phi^{-1} \left(1 - \frac{\delta}{8N_\epsilon} \right) \sigma_n$. Therefore, with probability at least $1 - \frac{\delta}{2N_\epsilon}$:

$$|\bar{\alpha}^\theta(\mathbf{x}|\mathcal{D}) - \alpha^{\theta+\epsilon_j}(\mathbf{x}|\mathcal{D})| \leq 2\Phi^{-1} \left(1 - \frac{\delta}{8N_\epsilon} \right) \sigma_n$$

Hence, by choosing $\sigma_n = \frac{\rho}{4\Phi^{-1} \left(1 - \frac{\delta}{8N_\epsilon} \right)}$ we arrive:

$$|\bar{\alpha}^\theta(\mathbf{x}|\mathcal{D}) - \alpha^{\theta+\epsilon_j}(\mathbf{x}|\mathcal{D})| \leq \frac{\rho}{2}$$

and, therefore, for the first term in (5) with probability at least $1 - \frac{\delta}{2}$ we have:

$$\frac{1}{N_\epsilon} \sum_{j=1}^{N_\epsilon} |\bar{\alpha}^\theta(\mathbf{x}|\mathcal{D}) - \alpha^{\theta+\epsilon_j}(\mathbf{x}|\mathcal{D})| \leq \frac{\rho}{2}$$

Combining this result with (6) gives, that with probability at least $1 - \delta$ we have:

$$|\bar{\alpha}^\theta(\mathbf{x}|\mathcal{D}) - \mathbb{E}_{\epsilon \sim \mathcal{N}(\mathbf{0}, \sigma_\epsilon^2 \mathbf{I})} [\alpha^{\theta+\epsilon}(\mathbf{x}|\mathcal{D})]| \leq \rho$$

upon the following setup:

$$\sigma_n = \frac{\rho}{4\Phi^{-1}\left(1 - \frac{\delta}{8N_\epsilon}\right)}, \quad (7)$$

$$\sigma_\epsilon = \min \left\{ 1, \frac{\rho}{8 \left[2\sqrt{p} + \sqrt{\log \frac{4N_\epsilon}{\delta}} \right] [A_1 + o(1)]} \right\},$$

with

$$N_\epsilon = \left\lceil \frac{16 \left[\mathbb{E}_\epsilon [\mu_{\theta+\epsilon}^2(\mathbf{x}|\mathcal{D})] + \frac{\beta\pi}{2} \mathbb{E}_\epsilon [\sigma_{\theta+\epsilon}^2(\mathbf{x}|\mathcal{D})] \right]}{\delta\rho^2} \right\rceil.$$

Our last step is to prove the existence of constant A_1 such that $\|\mathbf{h}_\theta(\mathbf{x})\|_2 \leq A_1$ and also to simplify these expressions by deriving bounds on $\mathbb{E}_\epsilon [\mu_{\theta+\epsilon}(\mathbf{x}|\mathcal{D})]$ and $\mathbb{E}_\epsilon [\sigma_{\theta+\epsilon}^2(\mathbf{x}|\mathcal{D})]$. This will be provided as a separate Claim:

Claim: Let bounds (4) are hold, then there are positive constants A_1, A_2 and A_3 , such that:

$$\|\mathbf{h}_\theta(\mathbf{x})\|_2 \leq A_1, \quad (8)$$

$$\mathbb{E}_\epsilon [\mu_{\theta+\epsilon}(\mathbf{x}|\mathcal{D})] \leq A_2, \quad \mathbb{E}_\epsilon [\sigma_{\theta+\epsilon}^2(\mathbf{x}|\mathcal{D})] \leq A_3.$$

Proof. We start with bound on $\|\mathbf{h}_\theta(\mathbf{x})\|_2$. Let us denote for simplicity $\mathbf{a}_\theta = [k_\theta(\mathbf{x}, \mathbf{x}_i)]_{\mathbf{x}_i \in \mathcal{D}}$, $\mathbf{B}_\theta = [k_\theta(\mathbf{x}, \mathbf{x}') + \mathbf{I}]_{\mathbf{x} \in \mathcal{D}, \mathbf{x}' \in \mathcal{D}}^{-1}$, $\mathbf{y} = [y(\mathbf{x})]_{\mathbf{x} \in \mathcal{D}}$, $\mathbf{m}_\mathcal{D} = [m(\mathbf{x})]_{\mathbf{x} \in \mathcal{D}}$, $m = m(\mathbf{x})$, and $k_\theta = k_\theta(\mathbf{x}, \mathbf{x})$, then

$$\mu_\theta(\mathbf{x}|\mathcal{D}) = \mathbf{a}_\theta^\top \mathbf{B}_\theta [\mathbf{y} - \mathbf{m}_\mathcal{D}] + m,$$

$$\sigma_\theta^2(\mathbf{x}|\mathcal{D}) = \mathbf{a}_\theta^\top \mathbf{B}_\theta \mathbf{a}_\theta + k_\theta$$

Let us also denote the size of \mathcal{D} as N , then: have:

$$\nabla_\theta \mu_\theta(\mathbf{x}|\mathcal{D}) = \sum_{i=1}^N \sum_{j=1}^N \nabla_\theta [[y_j - m_j][\mathbf{a}_\theta]_i [\mathbf{B}_\theta]_{ij}] =$$

$$\sum_{i=1}^N \sum_{j=1}^N [[y_j - m_j][\mathbf{B}_\theta]_{ij} \nabla_\theta [\mathbf{a}_\theta]_i] +$$

$$\sum_{i=1}^N \sum_{j=1}^N [[y_j - m_j][\mathbf{a}_\theta]_i \nabla_\theta [[\mathbf{B}_\theta]_{ij}]]$$

Consider each term in this expression separately:

$$\left\| \sum_{i=1}^N \sum_{j=1}^N [y_j - m_j][\mathbf{B}_\theta]_{ij} \nabla_\theta [\mathbf{a}_\theta]_i \right\|_2 =$$

$$\left\| \sum_{i=1}^N [\mathbf{B}_\theta [\mathbf{y} - \mathbf{m}_\mathcal{D}]]_i \nabla_\theta [\mathbf{a}_\theta]_i \right\|_2 \leq$$

$$\sum_{i=1}^N \|\mathbf{B}_\theta(i, :)\|_2 \|\mathbf{y} - \mathbf{m}_\mathcal{D}\|_2 \|\nabla_\theta [\mathbf{a}_\theta]_i\|_2$$

Using $|y| \leq C$ and $|m(\mathbf{x})| \leq M_4$ we have $\|\mathbf{y} - \mathbf{m}_\mathcal{D}\|_2 \leq (C + M_4)\sqrt{N}$ and $\|\nabla_\theta [\mathbf{a}_\theta]_i\|_2 \leq M_2$ we have:

$$\left\| \sum_{i=1}^N \sum_{j=1}^N [y_j - m_j][\mathbf{B}_\theta]_{ij} \nabla_\theta [\mathbf{a}_\theta]_i \right\|_2 \leq \quad (9)$$

$$(C + M_4)\sqrt{N} \sum_{i=1}^N \|\mathbf{B}_\theta(i, :)\|_2 \|\nabla_\theta [\mathbf{a}_\theta]_i\|_2 \leq$$

$$(C + M_4)\sqrt{N} \|\mathbf{B}_\theta\|_F \sum_{i=1}^N \|\nabla_\theta [\mathbf{a}_\theta]_i\|_2 \leq$$

$$(C + M_4)\sqrt{N} \sqrt{\text{rank}(\mathbf{B}_\theta) \|\mathbf{B}_\theta\|_2} \sum_{i=1}^N \|\nabla_\theta [\mathbf{a}_\theta]_i\|_2 \leq$$

$$\frac{(C + M_4)N}{\sigma_n^2} \sum_{i=1}^N \|\nabla_\theta [\mathbf{a}_\theta]_i\|_2 = \frac{(C + M_4)N^2 M_2}{\sigma_n^2}$$

Now, let us consider the second term in the expression for the posterior mean:

$$\sum_{i=1}^N \sum_{j=1}^N [y_j - m_j][\mathbf{a}_\theta]_i \nabla_\theta [[\mathbf{B}_\theta]_{ij}] =$$

$$\sum_{i=1}^N [\mathbf{a}_\theta]_i \left[\sum_{j=1}^N [y_j - m_j] \nabla_\theta [[\mathbf{B}_\theta]_{ij}] \right]$$

Notice, that the gradient expression above is presented in a form of a vector:

$$\nabla_\theta [[\mathbf{B}_\theta]_{ij}] = \begin{bmatrix} \frac{\partial}{\partial \theta_1} [\mathbf{K}_\theta + \sigma_n \mathbf{I}]_{ij}^{-1}, \\ \vdots \\ \frac{\partial}{\partial \theta_p} [\mathbf{K}_\theta + \sigma_n \mathbf{I}]_{ij}^{-1} \end{bmatrix}$$

where we use notation $\mathbf{K}_\theta = [k_\theta(\mathbf{x}_i, \mathbf{x}_j)]_{i=1, j=1}^{N, N}$. For the r^{th} component we have:

$$\frac{\partial}{\partial \theta_r} [\mathbf{K}_\theta + \sigma_n \mathbf{I}]_{ij}^{-1} = \quad (10)$$

$$\left[-[\mathbf{K}_\theta + \sigma_n \mathbf{I}]^{-1} \frac{\partial}{\partial \theta_r} [\mathbf{K}_\theta + \sigma_n \mathbf{I}] [\mathbf{K}_\theta + \sigma_n \mathbf{I}]^{-1} \right]_{ij}$$

Now we can study the gradient of the second term in the posterior mean expression:

$$\left\| \sum_{i=1}^N [\mathbf{a}_\theta]_i \left[\sum_{j=1}^N [y_j - m_j] \nabla_\theta [[\mathbf{B}_\theta]_{ij}] \right] \right\|_2 \leq$$

$$\sum_{i=1}^N \|[\mathbf{a}_\theta]_i\| \left[\sum_{j=1}^N \|\mathbf{y} - \mathbf{m}_\mathcal{D}\|_2 \|\nabla_\theta [[\mathbf{B}_\theta]_{ij}]\|_2 \right] \leq$$

$$(C + M_4)\sqrt{N} M_1 \sum_{i=1}^N \sum_{j=1}^N \sum_{r=1}^p \left| \frac{\partial}{\partial \theta_r} [\mathbf{K}_\theta + \sigma_n \mathbf{I}]_{ij}^{-1} \right|$$

Using result (10) in the above expression we have:

$$\begin{aligned}
 & \left\| \sum_{i=1}^N [\mathbf{a}_\theta]_i \left[\sum_{j=1}^N [y_j - m_j] \nabla_\theta [[\mathbf{B}_\theta]_{ij}] \right] \right\|_2 \leq \\
 & (C + M_4) \sqrt{N} M_1 \sum_{i=1}^N \sum_{j=1}^N \sum_{r=1}^p \left| \frac{\partial}{\partial \theta_r} [\mathbf{K}_\theta + \sigma_n \mathbf{I}]_{ij}^{-1} \right| \leq \\
 & (C + M_4) \sqrt{N} M_1 \sum_{r=1}^p \sum_{i=1}^N \sum_{j=1}^N \left| \frac{\partial}{\partial \theta_r} [\mathbf{K}_\theta + \sigma_n \mathbf{I}]_{ij}^{-1} \right| \leq \\
 & (C + M_4) N \sqrt{N} M_1 \times \\
 & \sum_{r=1}^p \left\| [\mathbf{K}_\theta + \sigma_n \mathbf{I}]^{-1} \frac{\partial}{\partial \theta_r} [\mathbf{K}_\theta + \sigma_n \mathbf{I}] [\mathbf{K}_\theta + \sigma_n \mathbf{I}]^{-1} \right\|_F
 \end{aligned}$$

where we used that $\sum_{i=1}^N \sum_{j=1}^N |\mathbf{C}_{ij}| \leq N \|\mathbf{C}\|_F$ for any arbitrary matrix $\mathbf{C} \in \mathbb{R}^{N \times N}$. Because $\frac{\partial}{\partial \theta_r} [\mathbf{K}_\theta + \sigma_n \mathbf{I}] = \frac{\partial}{\partial \theta_r} \mathbf{K}_\theta$. Therefore:

$$\begin{aligned}
 & \frac{\left\| \sum_{i=1}^N [\mathbf{a}_\theta]_i \left[\sum_{j=1}^N [y_j - m_j] \nabla_\theta [[\mathbf{B}_\theta]_{ij}] \right] \right\|_2}{(C + M_4) N \sqrt{N} M_1} \leq \\
 & \sum_{r=1}^p \left\| [\mathbf{K}_\theta + \sigma_n \mathbf{I}]^{-1} \frac{\partial}{\partial \theta_r} \mathbf{K}_\theta [\mathbf{K}_\theta + \sigma_n \mathbf{I}]^{-1} \right\|_F \leq \\
 & \sqrt{N} \sum_{r=1}^p \left\| [\mathbf{K}_\theta + \sigma_n \mathbf{I}]^{-1} \frac{\partial}{\partial \theta_r} \mathbf{K}_\theta [\mathbf{K}_\theta + \sigma_n \mathbf{I}]^{-1} \right\|_2
 \end{aligned}$$

Using properties of matrix 2-norm $\|\cdot\|_2$:

$$\left\| [\mathbf{K}_\theta + \sigma_n \mathbf{I}]^{-1} \right\|_2 \leq \frac{1}{\sigma_n^2}$$

Hence,

$$\begin{aligned}
 & \frac{\left\| \sum_{i=1}^N [\mathbf{a}_\theta]_i \left[\sum_{j=1}^N [y_j - m_j] \nabla_\theta [[\mathbf{B}_\theta]_{ij}] \right] \right\|_2}{(C + M_4) N^2 M_1} \leq \quad (11) \\
 & \sum_{r=1}^p \left\| [\mathbf{K}_\theta + \sigma_n \mathbf{I}]^{-1} \right\|_2 \left\| \frac{\partial}{\partial \theta_r} \mathbf{K}_\theta \right\|_2 \left\| [\mathbf{K}_\theta + \sigma_n \mathbf{I}]^{-1} \right\|_2 \leq \\
 & \frac{1}{\sigma_n^4} \sum_{r=1}^p \left\| \frac{\partial}{\partial \theta_r} \mathbf{K}_\theta \right\|_2.
 \end{aligned}$$

Let us study the last term in the above expression. Using $\sqrt{c_1^2 + \dots + c_R^2} \leq |c_1| + \dots + |c_R|$ for any set of real

numbers $c_1, \dots, c_R \in \mathbb{R}$ we have:

$$\begin{aligned}
 & \left\| \frac{\partial}{\partial \theta_r} \mathbf{K}_\theta \right\|_2 = \\
 & \left\| \begin{bmatrix} \frac{\partial}{\partial \theta_r} k_\theta(\mathbf{x}_1, \mathbf{x}_1), & \dots & \frac{\partial}{\partial \theta_r} k_\theta(\mathbf{x}_1, \mathbf{x}_N) \\ \vdots & \ddots & \vdots \\ \frac{\partial}{\partial \theta_r} k_\theta(\mathbf{x}_N, \mathbf{x}_1), & \dots & \frac{\partial}{\partial \theta_r} k_\theta(\mathbf{x}_N, \mathbf{x}_N) \end{bmatrix} \right\|_2 \leq \\
 & \left\| \begin{bmatrix} \frac{\partial}{\partial \theta_r} k_\theta(\mathbf{x}_1, \mathbf{x}_1), & \dots & \frac{\partial}{\partial \theta_r} k_\theta(\mathbf{x}_1, \mathbf{x}_N) \\ \vdots & \ddots & \vdots \\ \frac{\partial}{\partial \theta_r} k_\theta(\mathbf{x}_N, \mathbf{x}_1), & \dots & \frac{\partial}{\partial \theta_r} k_\theta(\mathbf{x}_N, \mathbf{x}_N) \end{bmatrix} \right\|_F = \\
 & \sqrt{\sum_{i=1}^N \sum_{j=1}^N \left[\frac{\partial}{\partial \theta_r} k_\theta(\mathbf{x}_i, \mathbf{x}_j) \right]^2} \leq \sum_{i=1}^N \sum_{j=1}^N \left| \frac{\partial}{\partial \theta_r} k_\theta(\mathbf{x}_i, \mathbf{x}_j) \right|
 \end{aligned}$$

Substituting this expression in (11) gives us:

$$\frac{\left\| \sum_{i=1}^N [\mathbf{a}_\theta]_i \left[\sum_{j=1}^N [y_j - m_j] \nabla_\theta [[\mathbf{B}_\theta]_{ij}] \right] \right\|_2}{(C + M_4) N^2 M_1} \leq \quad (12)$$

$$\begin{aligned}
 & \frac{1}{\sigma_n^4} \sum_{r=1}^d \sum_{i=1}^N \sum_{j=1}^N \left| \frac{\partial}{\partial \theta_r} k_\theta(\mathbf{x}_i, \mathbf{x}_j) \right| \leq \\
 & \frac{\sqrt{p}}{\sigma_n^4} \sum_{i=1}^N \sum_{j=1}^N \|\nabla_\theta k_\theta(\mathbf{x}_i, \mathbf{x}_j)\|_2 \leq \frac{N^2 \sqrt{p} M_2}{\sigma_n^4}.
 \end{aligned}$$

Hence, combining results (9) and (12) we have:

$$\|\nabla_\theta \mu_\theta(\mathbf{x}|\mathcal{D})\|_2 \leq \frac{(C + M_4) N^2 M_2}{\sigma_n^2} \left[1 + \frac{N^2 M_1 \sqrt{p}}{\sigma_n^2} \right] \quad (13)$$

Now, let us focus on the gradient of the posterior deviation:

$$\nabla_\theta \sigma_\theta(\mathbf{x}|\mathcal{D}) = \quad (14)$$

$$\begin{aligned}
 & \nabla_\theta \left[\sqrt{k_\theta(\mathbf{x}, \mathbf{x}) - \mathbf{a}_\theta^\top [\mathbf{K}_\theta + \sigma_n^2 \mathbf{I}]^{-1} \mathbf{a}_\theta} \right] = \\
 & \frac{1}{2\sigma_\theta(\mathbf{x}|\mathcal{D})} \nabla_\theta [k_\theta(\mathbf{x}, \mathbf{x}) - \mathbf{a}_\theta^\top [\mathbf{K}_\theta + \sigma_n^2 \mathbf{I}]^{-1} \mathbf{a}_\theta] = \\
 & \frac{1}{2\sigma_\theta(\mathbf{x})} [\nabla_\theta k_\theta(\mathbf{x}, \mathbf{x}) - \nabla_\theta [\mathbf{a}_\theta^\top [\mathbf{K}_\theta + \sigma_n^2 \mathbf{I}]^{-1} \mathbf{a}_\theta]]
 \end{aligned}$$

Let us study the second gradient expression. Using or notation we have:

$$\begin{aligned}
 & \mathbf{a}_\theta^\top [\mathbf{K}_\theta + \sigma_n^2 \mathbf{I}]^{-1} \mathbf{a}_\theta = \\
 & \mathbf{a}_\theta^\top \mathbf{B}_\theta \mathbf{a}_\theta = \sum_{i=1}^N \sum_{j=1}^N [\mathbf{a}_\theta]_i [\mathbf{a}_\theta]_j [\mathbf{B}_\theta]_{ij}
 \end{aligned}$$

Hence, for the gradient we have:

$$\begin{aligned} \nabla_{\theta} [\mathbf{a}_{\theta}^{\top} \mathbf{B}_{\theta} \mathbf{a}_{\theta}] &= \sum_{i=1}^N \sum_{j=1}^N \nabla_{\theta} \left[[\mathbf{a}_{\theta}]_i [\mathbf{a}_{\theta}]_j [\mathbf{B}_{\theta}]_{ij} \right] = \\ &\sum_{i=1}^N \sum_{j=1}^N \nabla_{\theta} \left[[\mathbf{a}_{\theta}]_i [\mathbf{a}_{\theta}]_j [\mathbf{B}_{\theta}]_{ij} \right] + \\ &\sum_{i=1}^N \sum_{j=1}^N \nabla_{\theta} \left[[\mathbf{a}_{\theta}]_j [\mathbf{a}_{\theta}]_i [\mathbf{B}_{\theta}]_{ij} \right] + \\ &\sum_{i=1}^N \sum_{j=1}^N \nabla_{\theta} \left[[\mathbf{B}_{\theta}]_{ij} \right] [\mathbf{a}_{\theta}]_i [\mathbf{a}_{\theta}]_j. \end{aligned}$$

Hence, for the norm of the above expression we have:

$$\begin{aligned} \|\nabla_{\theta} [\mathbf{a}_{\theta}^{\top} \mathbf{B}_{\theta} \mathbf{a}_{\theta}]\|_2 &= \sum_{i=1}^N \sum_{j=1}^N \nabla_{\theta} \left[[\mathbf{a}_{\theta}]_i [\mathbf{a}_{\theta}]_j [\mathbf{B}_{\theta}]_{ij} \right] = \\ &\sum_{i=1}^N \sum_{j=1}^N \left\| \nabla_{\theta} \left[[\mathbf{B}_{\theta}]_{ij} \right] \right\|_2 \left| [\mathbf{a}_{\theta}]_i [\mathbf{a}_{\theta}]_j \right| + \\ &\sum_{i=1}^N \sum_{j=1}^N \|\nabla_{\theta}\|_2 \left| [\mathbf{a}_{\theta}]_i [\mathbf{a}_{\theta}]_j [\mathbf{B}_{\theta}]_{ij} \right| + \\ &\sum_{i=1}^N \sum_{j=1}^N \|\nabla_{\theta} [[\mathbf{a}_{\theta}]_j]\|_2 \left| [\mathbf{a}_{\theta}]_i [\mathbf{B}_{\theta}]_{ij} \right|. \end{aligned}$$

Let us bound each term in this expression:

1. The first term:

$$\begin{aligned} &\sum_{i=1}^N \sum_{j=1}^N \left\| \nabla_{\theta} \left[[\mathbf{B}_{\theta}]_{ij} \right] \right\|_2 \left| [\mathbf{a}_{\theta}]_i [\mathbf{a}_{\theta}]_j \right| \leq \\ &\sum_{i=1}^N \sum_{j=1}^N \left\| \nabla_{\theta} \left[[\mathbf{B}_{\theta}]_{ij} \right] \right\|_2 \|\mathbf{a}_{\theta}\|_2 \|\mathbf{a}_{\theta}\|_2 \leq \\ &M_1^2 \sum_{i=1}^N \sum_{j=1}^N \left\| \nabla_{\theta} \left[[\mathbf{B}_{\theta}]_{ij} \right] \right\|_2 \end{aligned}$$

Using previous bound for $\left\| \nabla_{\theta} \left[[\mathbf{B}_{\theta}]_{ij} \right] \right\|_2$ we have:

$$\begin{aligned} &\sum_{i=1}^N \sum_{j=1}^N \left\| \nabla_{\theta} \left[[\mathbf{B}_{\theta}]_{ij} \right] \right\|_2 \left| [\mathbf{a}_{\theta}]_i [\mathbf{a}_{\theta}]_j \right| \leq \\ &M_1^2 \sum_{i=1}^N \sum_{j=1}^N \sum_{r=1}^p \left| \frac{\partial}{\partial \theta_r} [\mathbf{K}_{\theta} + \sigma_n^2 \mathbf{I}]_{ij}^{-1} \right| = \\ &N M_1^2 \sum_{r=1}^p \left\| [\mathbf{K}_{\theta} + \sigma_n \mathbf{I}]^{-1} \frac{\partial}{\partial \theta_r} \mathbf{K}_{\theta} [\mathbf{K}_{\theta} + \sigma_n \mathbf{I}]^{-1} \right\|_F \leq \\ &N^{\frac{3}{2}} M_1^2 \sum_{r=1}^p \left\| [\mathbf{K}_{\theta} + \sigma_n \mathbf{I}]^{-1} \frac{\partial}{\partial \theta_r} \mathbf{K}_{\theta} [\mathbf{K}_{\theta} + \sigma_n \mathbf{I}]^{-1} \right\|_2 \end{aligned}$$

Since $\left\| [\mathbf{K}_{\theta} + \sigma_n \mathbf{I}]^{-1} \right\|_2 \leq \frac{1}{\sigma_n^2}$ we have:

$$\begin{aligned} &\sum_{i=1}^N \sum_{j=1}^N \left\| \nabla_{\theta} \left[[\mathbf{B}_{\theta}]_{ij} \right] \right\|_2 \left| [\mathbf{a}_{\theta}]_i [\mathbf{a}_{\theta}]_j \right| \leq \\ &\frac{N \sqrt{N} M_1^2}{\sigma_n^4} \sum_{r=1}^p \sum_{i=1}^N \sum_{j=1}^N \left| \frac{\partial}{\partial \theta_r} k_{\theta}(\mathbf{x}_i, \mathbf{x}_j) \right|. \end{aligned}$$

Using $\sum_{r=1}^p \sum_{i=1}^N \sum_{j=1}^N \left| \frac{\partial}{\partial \theta_r} k_{\theta}(\mathbf{x}_i, \mathbf{x}_j) \right| = \sqrt{p} \sum_{i=1}^N \sum_{j=1}^N \|\nabla_{\theta} k_{\theta}(\mathbf{x}_i, \mathbf{x}_j)\|_2 \leq N^2 \sqrt{p} M_2$, we have:

$$\sum_{i=1}^N \sum_{j=1}^N \left\| \nabla_{\theta} \left[[\mathbf{B}_{\theta}]_{ij} \right] \right\|_2 \left| [\mathbf{a}_{\theta}]_i [\mathbf{a}_{\theta}]_j \right| \leq \frac{N^{\frac{7}{2}} \sqrt{p} M_1^2 M_2}{\sigma_n^4}$$

2. The second and the third terms are identical with respect to bounding strategy:

$$\begin{aligned} &\sum_{i=1}^N \sum_{j=1}^N \|\nabla_{\theta} [[\mathbf{a}_{\theta}]_i]\|_2 \left| [\mathbf{a}_{\theta}]_j [\mathbf{B}_{\theta}]_{ij} \right| = \\ &\sum_{i=1}^N |\mathbf{B}_{\theta}(i, :)\mathbf{a}_{\theta}| \|\nabla_{\theta} [[\mathbf{a}_{\theta}]_i]\|_2 \leq \\ &\sum_{i=1}^N \|\mathbf{B}_{\theta}(i, :)\|_2 \|\mathbf{a}_{\theta}\|_2 \|\nabla_{\theta} [[\mathbf{a}_{\theta}]_i]\|_2 \leq \\ &\|\mathbf{B}_{\theta}\|_F \|\mathbf{a}_{\theta}\|_2 \sum_{i=1}^N \|\nabla_{\theta} [[\mathbf{a}_{\theta}]_i]\|_2 \end{aligned}$$

Since $\|\mathbf{B}_{\theta}\|_F \leq \sqrt{\text{rank}(\mathbf{B}_{\theta})} \|\mathbf{B}_{\theta}\|_2 \leq \frac{\sqrt{N}}{\sigma_n^2}$. Hence,

$$\sum_{i=1}^N \sum_{j=1}^N \|\nabla_{\theta} [[\mathbf{a}_{\theta}]_i]\|_2 \left| [\mathbf{a}_{\theta}]_j [\mathbf{B}_{\theta}]_{ij} \right| \leq \frac{N \sqrt{N} M_1 M_2}{\sigma_n^2}$$

Combining these results and using $\|\nabla_{\theta} k_{\theta}(\mathbf{x}, \mathbf{x})\| \leq M_2$, $|\sigma_{\theta}(\mathbf{x}|\mathcal{D})| \geq k_{\theta}(\mathbf{x}, \mathbf{x}) \geq M_0$, we have:

$$\|\nabla_{\theta} [\sigma_{\theta}(\mathbf{x}|\mathcal{D})]\|_2 \leq \frac{N \sqrt{N} M_1 M_2}{2 \sigma_n^2 M_0} \left[\frac{N^2 \sqrt{p} M_1}{\sigma_n^2} + 2 \right] \quad (15)$$

Hence, combining (13) and (15) we have:

$$\begin{aligned} \|\mathbf{h}_{\theta}(\mathbf{x}|\mathcal{D})\|_2 &\leq \\ \|\nabla_{\theta} \mu_{\theta}(\mathbf{x}|\mathcal{D})\|_2 &+ \sqrt{\frac{\beta \pi}{2}} \|\nabla_{\theta} [\sigma_{\theta}(\mathbf{x}|\mathcal{D})]\|_2 \leq \\ &\frac{(C + M_4) N^2 M_2}{\sigma_n^2} \left[1 + \frac{N^2 M_1 \sqrt{p}}{\sigma_n^2} \right] + \\ &\sqrt{\frac{\beta \pi}{2}} \frac{N \sqrt{N} M_1 M_2}{2 \sigma_n^2 M_0} \left[\frac{N^2 \sqrt{p} M_1}{\sigma_n^2} + 2 \right] \triangleq A_1. \end{aligned}$$

Now, we are ready to bound the other two terms in the claim:

$$\begin{aligned} \mu_{\theta+\epsilon}^2(\mathbf{x}|\mathcal{D}) &\leq 2 [\mathbf{a}_{\theta+\epsilon}^\top \mathbf{B}_{\theta+\epsilon} [\mathbf{y} - \mathbf{m}_{\mathcal{D}}]]^2 + 2|m|^2 \leq \\ &2 \frac{(C + M_4)^2 M_1^2}{\sigma_n^4} + 2M_4^2 \end{aligned}$$

Therefore, for $\mathbb{E}_\epsilon [\mu_{\theta+\epsilon}^2(\mathbf{x}|\mathcal{D})]$ we have:

$$\mathbb{E}_\epsilon [\mu_{\theta+\epsilon}^2(\mathbf{x}|\mathcal{D})] \leq 2 \frac{(C + M_4)^2 M_1^2}{\sigma_n^4} + 2M_4^2 \triangleq A_2.$$

Finally, for the posterior mean:

$$\begin{aligned} \sigma_{\theta+\epsilon}^2(\mathbf{x}|\mathcal{D}) &\leq k_\theta(\mathbf{x}, \mathbf{x}) + \mathbf{a}_{\theta+\epsilon}^\top \mathbf{B}_{\theta+\epsilon} \mathbf{a}_{\theta+\epsilon} \leq \\ &M_1 + \frac{M_1^2}{\sigma_n^2} \end{aligned}$$

Therefore, for $\mathbb{E}_\epsilon [\sigma_{\theta+\epsilon}^2(\mathbf{x}|\mathcal{D})]$ we have:

$$\mathbb{E}_\epsilon [\sigma_{\theta+\epsilon}^2(\mathbf{x}|\mathcal{D})] \leq M_1 + \frac{M_1^2}{\sigma_n^2} \triangleq A_3.$$

This finishes the proof of the claim. \square

Having equipped with these results, we can further simplify the setup expressions (7):

$$\begin{aligned} \sigma_n &= \frac{\rho}{4\Phi^{-1}\left(1 - \frac{\delta}{8N_\epsilon}\right)}, \\ \sigma_\epsilon &= \min \left\{ 1, \frac{\rho}{8 \left[2\sqrt{p} + \sqrt{\log \frac{4N_\epsilon}{\delta}} \right] [A_1 + o(1)]} \right\}, \end{aligned}$$

with

$$N_\epsilon = \left\lceil \frac{16 \left[A_2 + \frac{\beta\pi}{2} A_3 \right]}{\delta\rho^2} \right\rceil.$$

This finishes the proof of the lemma. \square

D. Acquisition function conflicts

The full set of experiments described in section 3.3 highlighting conflicts of widely used acquisition functions can be visualised on Figures 7-12. For each plot, respective maximisers of EI, PI and UCB are shown with vertical lines to clearly indicate when optimising different acquisition functions leads to conflicting recommendations.

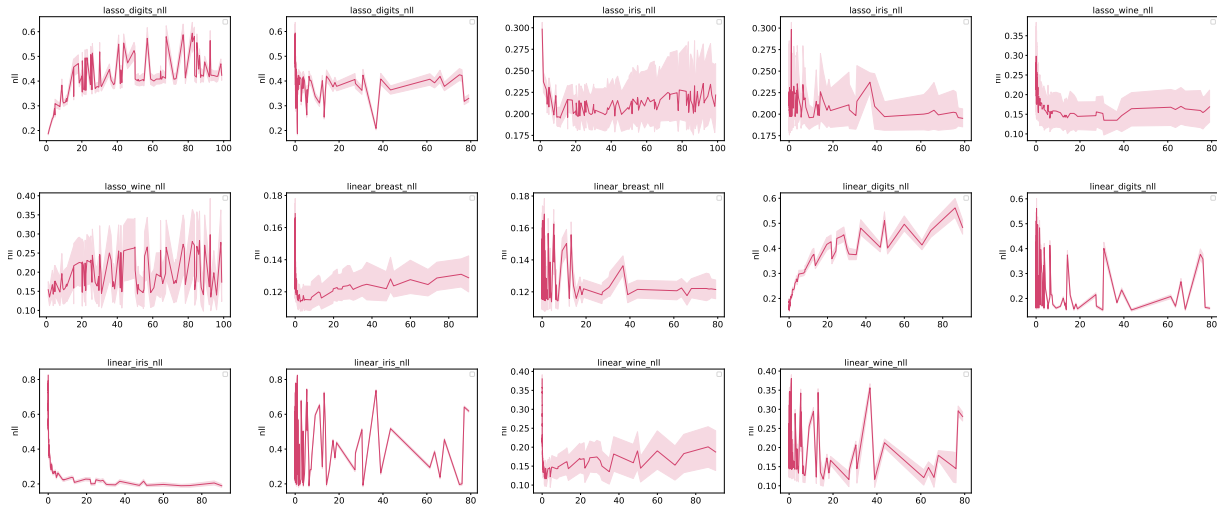


Figure 6. These figures show for several tasks the evolution of the observed noise level as hyperparameter values vary. Changes in the standard deviation magnitude (represented by the shaded areas) indicate that the noise level depends on the hyperparameter value, in other words they indicate heteroscedasticity. Drastic changes in standard deviation level are notably observed for (Lasso, Iris, NLL) or (Linear, Digits, NLL) tasks.

Table 4. Non-stationarity test on tasks involving Wine dataset. Log-probabilities on the held-out test set comprised of 32 points is reported for GP equipped with Matern-3/2 kernel (stationary) and Spectral Mixture kernel (non-stationary).

Dataset	Model	Metrics	Nonstationary kernel	Stationary kernel
wine	DT	acc	-4.86e+02	-1.25e+03
	MLP-adam	acc	-3.27e+01	-2.81e+02
	MLP-sgd	acc	-2.80e+01	-7.95e+02
	RF	acc	-1.43e+03	-8.26e+02
	ada	acc	2.12e+01	-1.27e+02
	kNN	acc	-1.27e+02	-1.24e+02
	lasso	acc	-1.32e+01	1.02e+02
	linear	acc	5.60e+01	7.30e+01
	DT	nll	-2.39e+03	-5.45e+02
	MLP-adam	nll	-6.37e+02	-1.54e+02
	MLP-sgd	nll	-4.81e+02	-1.41e+02
	RF	nll	-1.35e+04	-8.36e+02
	ada	nll	-4.33e+03	-1.85e+03
	kNN	nll	-6.48e+05	-6.54e+05
	lasso	nll	-4.27e+02	-2.96e+02
	linear	nll	-3.95e+00	1.71e+01

Generalised Bayesian Optimisation

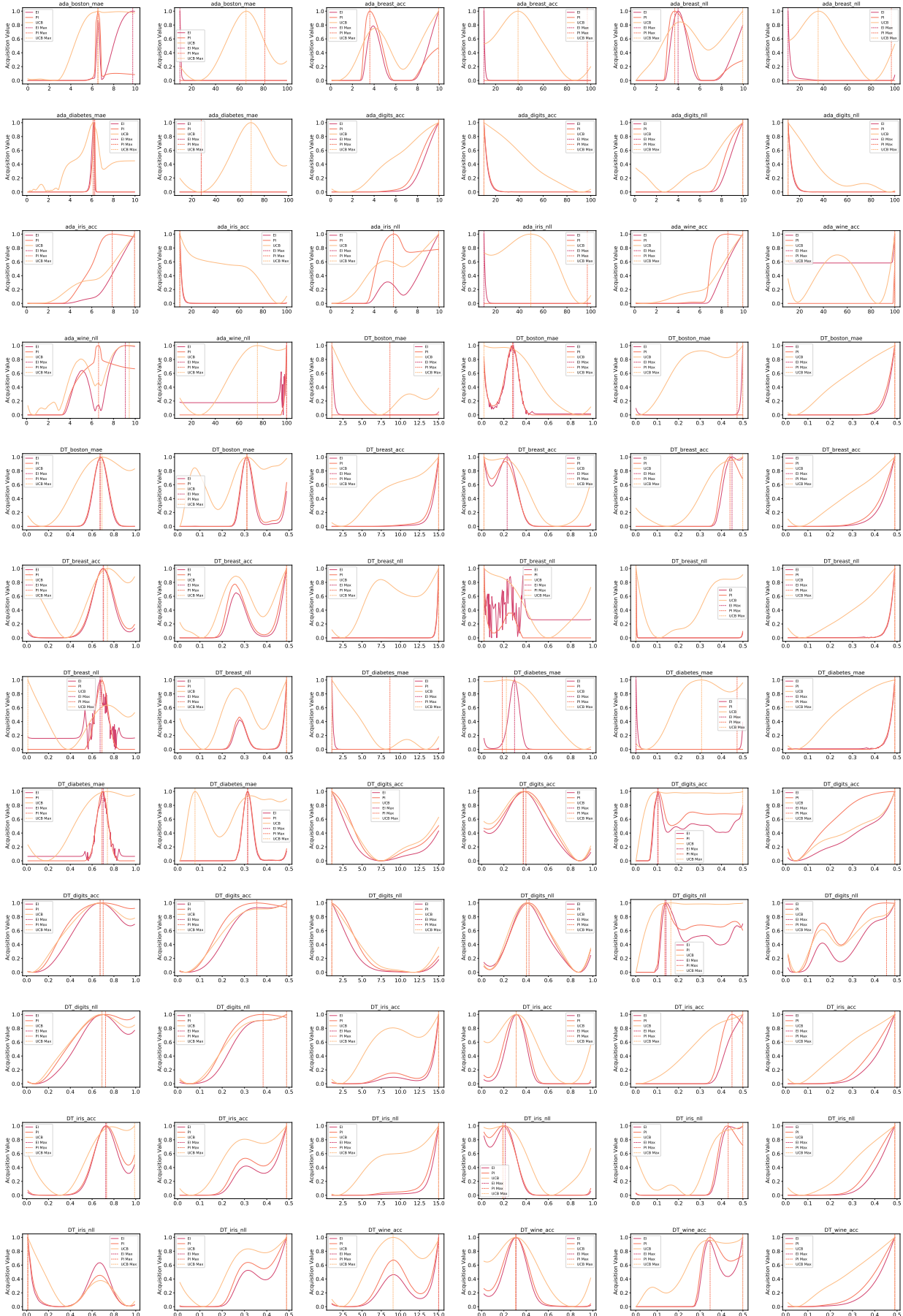


Figure 7. Conflicting acquisition functions

Generalised Bayesian Optimisation

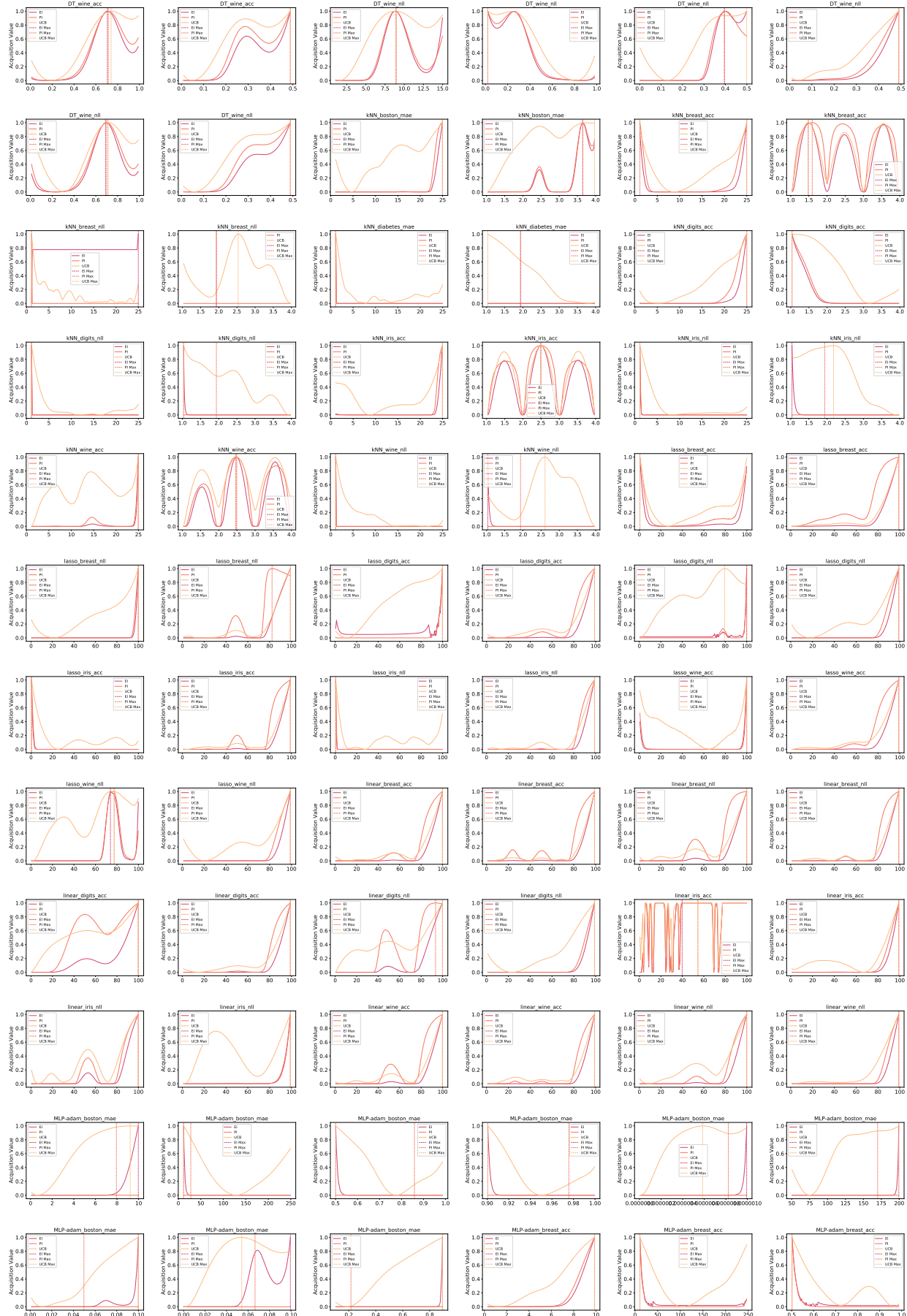


Figure 8. Conflicting acquisition functions

Generalised Bayesian Optimisation

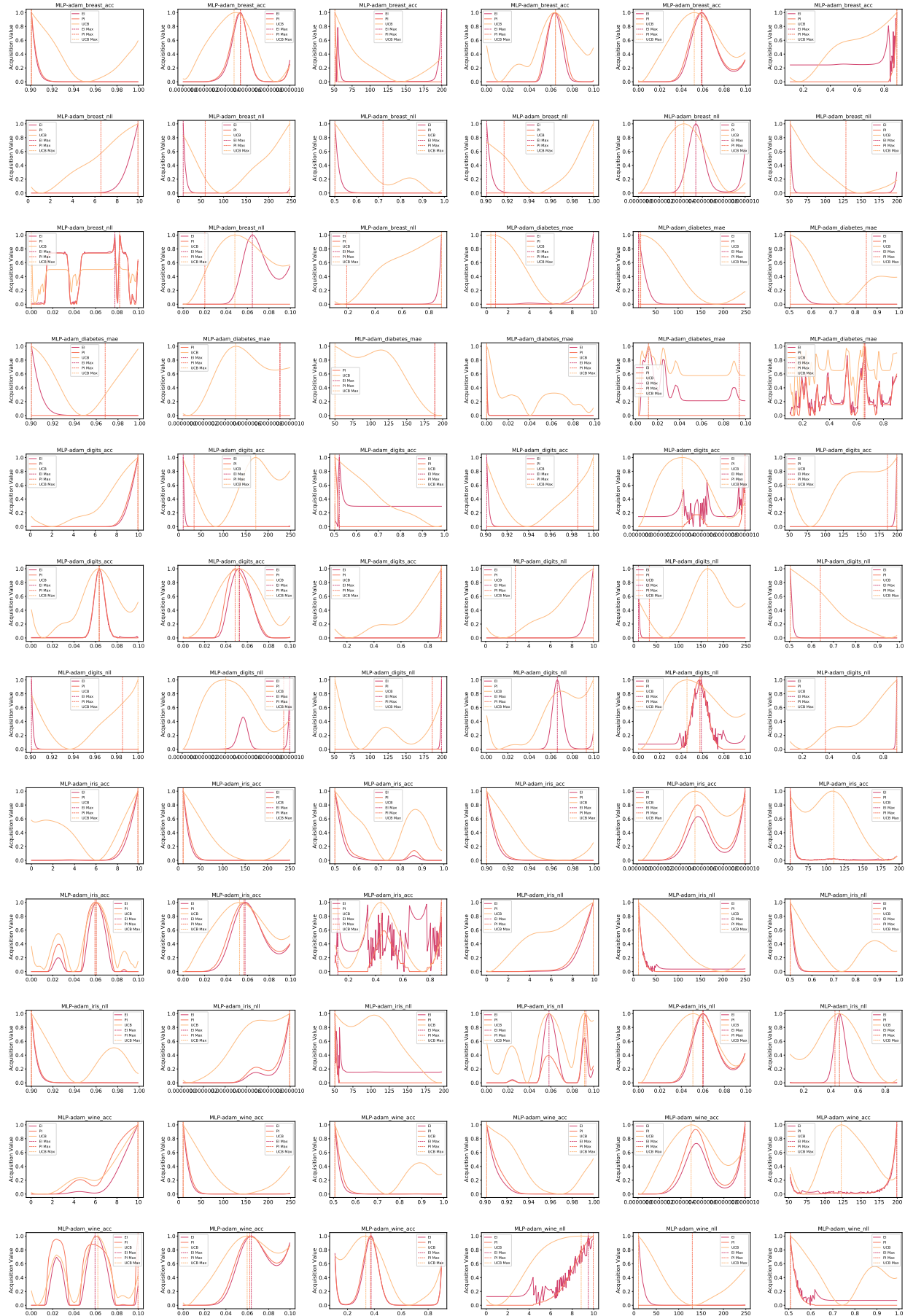


Figure 9. Conflicting acquisition functions

Generalised Bayesian Optimisation

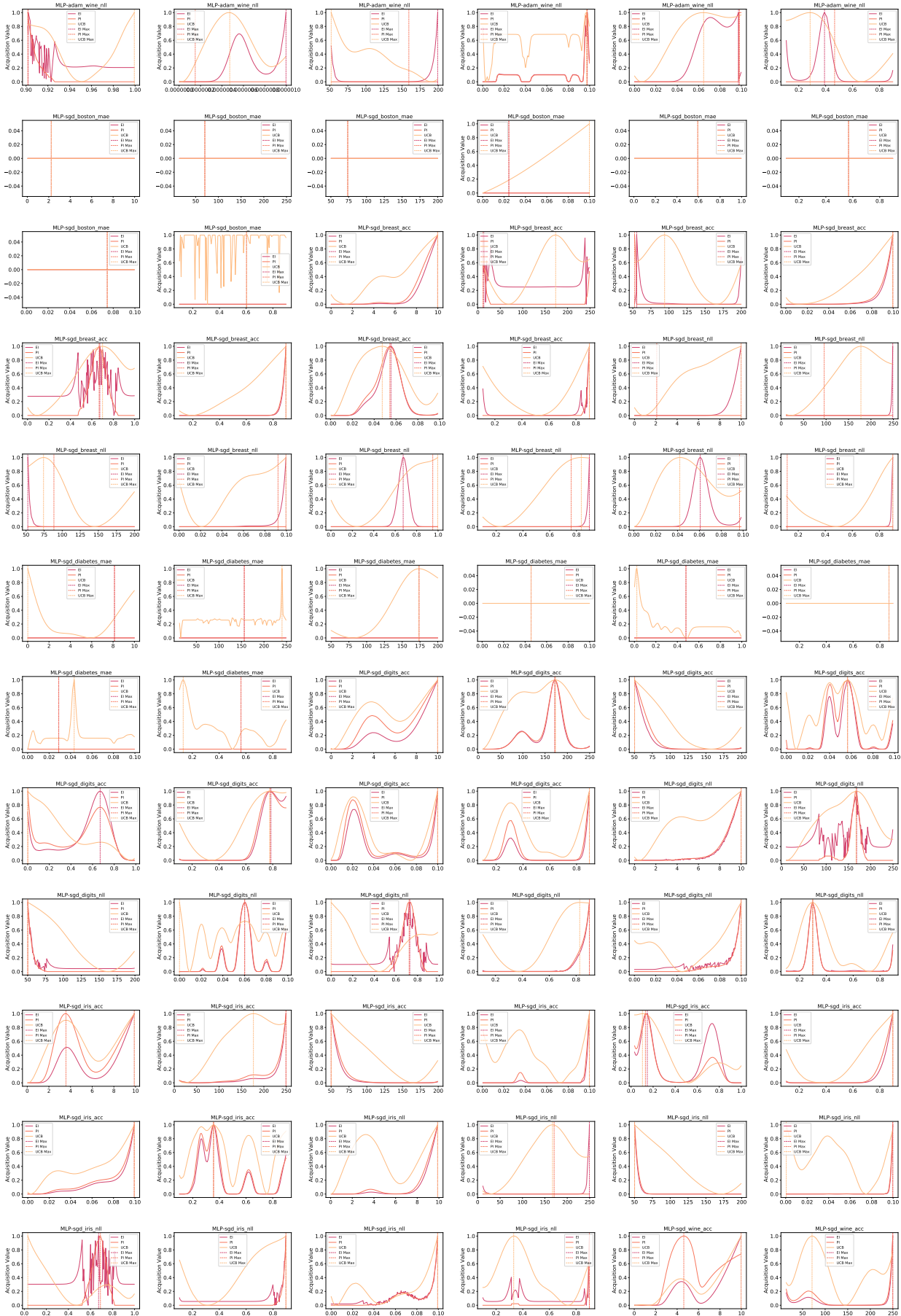


Figure 10. Conflicting acquisition functions

Generalised Bayesian Optimisation

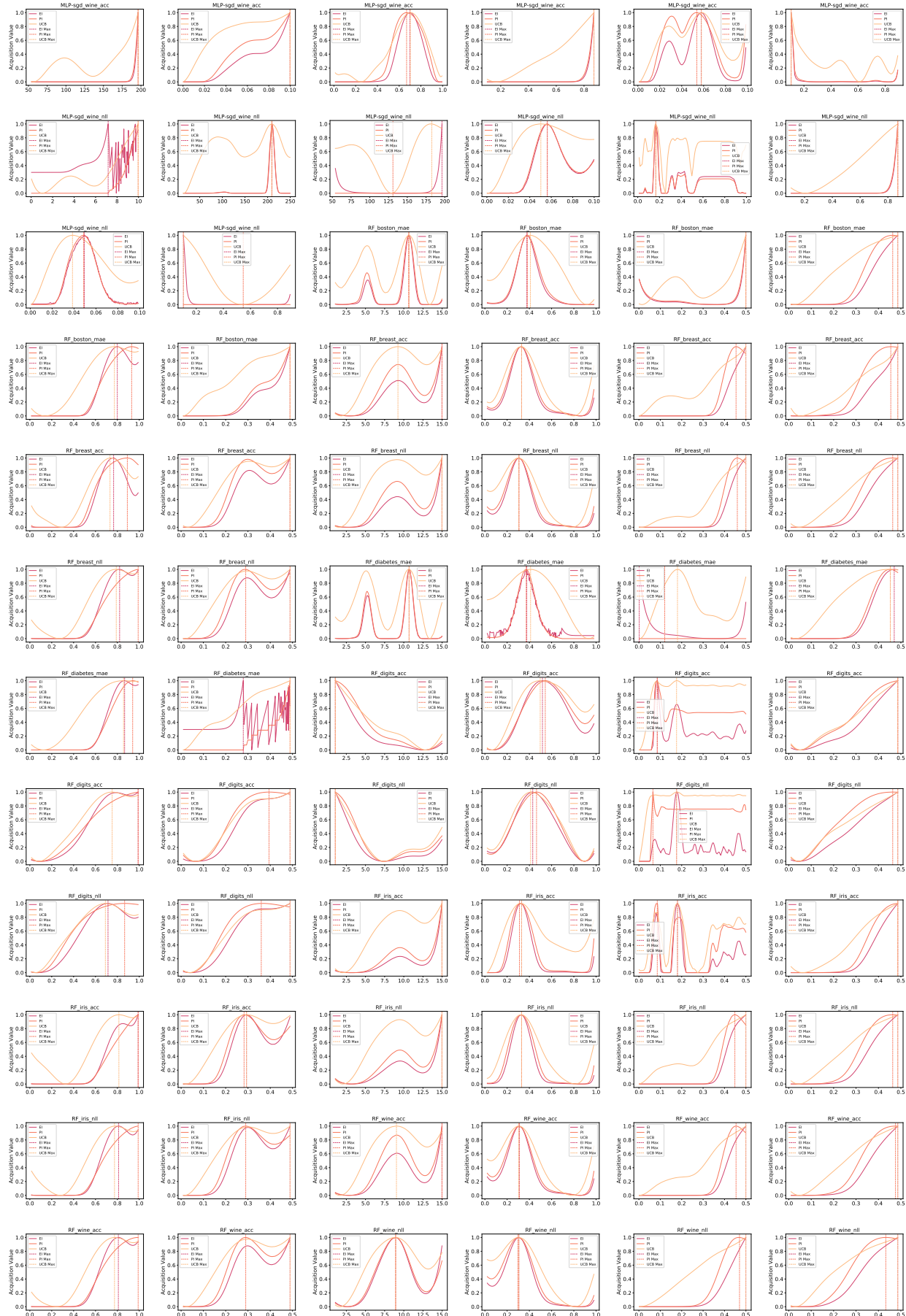


Figure 11. Conflicting acquisition functions

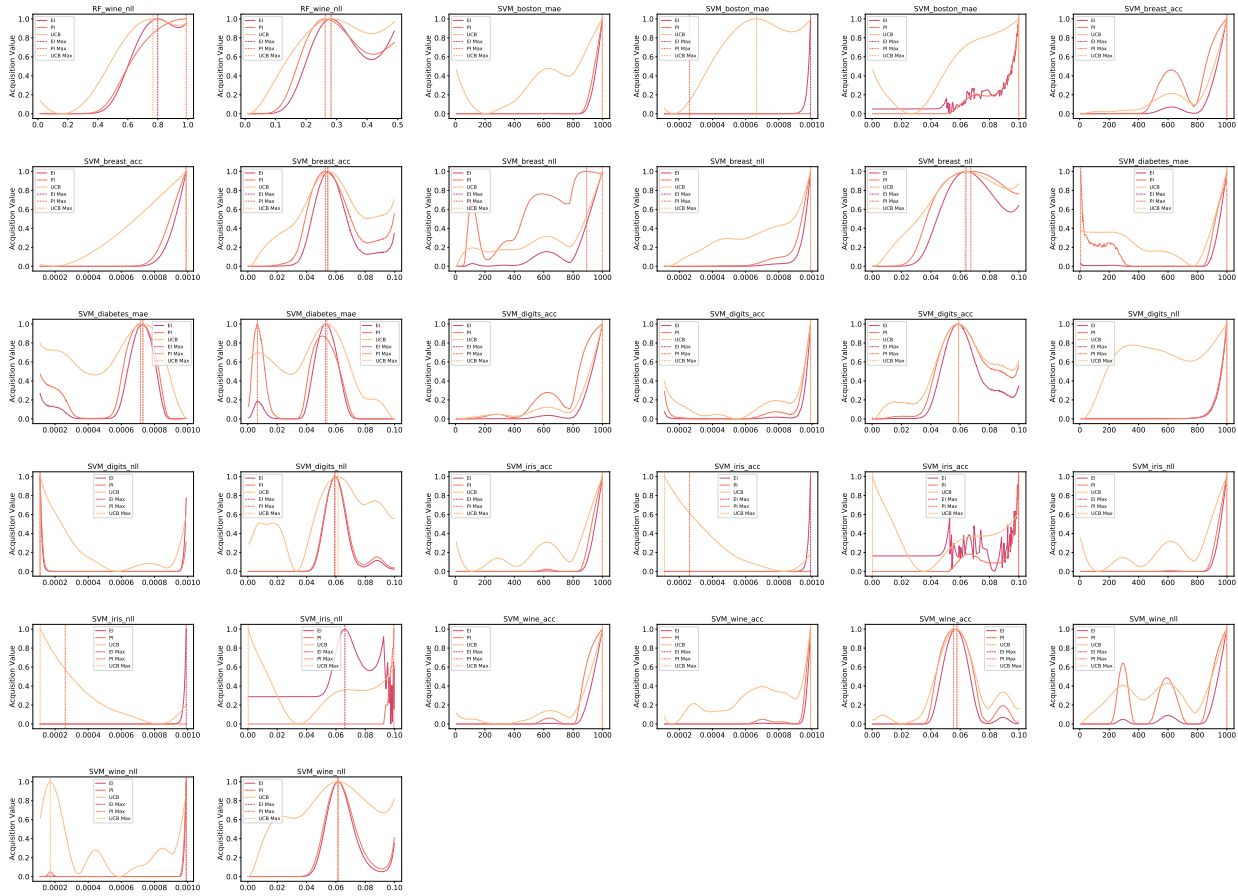


Figure 12. Conflicting acquisition functions

Table 5. Non-stationarity test on tasks involving Breast dataset

Dataset	Model	Metrics	Nonstationary kernel	Stationary kernel
breast	DT	acc	-1.88e+04	-5.26e+02
	MLP-adam	acc	-2.26e+05	-3.04e+02
	MLP-sgd	acc	-3.52e+05	-1.84e+02
	RF	acc	-4.27e+04	-7.42e+02
	ada	acc	-3.53e+03	-7.13e+03
	kNN	acc	1.06e+02	1.14e+02
	lasso	acc	-1.32e+01	1.43e+02
	linear	acc	8.39e+01	1.01e+02
	DT	nll	9.20e+00	-9.23e+02
	MLP-adam	nll	-6.45e+02	-1.65e+02
	MLP-sgd	nll	-5.71e+02	-1.60e+02
	RF	nll	-3.75e+02	-7.01e+02
	ada	nll	-8.18e+02	-3.05e+03
	kNN	nll	-7.57e+04	-7.58e+04
	lasso	nll	-1.45e+03	2.50e+01
	linear	nll	1.79e+01	2.14e+01

Table 6. Non-stationarity test on tasks involving `Boston` dataset

Dataset	Model	Metrics	Nonstationary kernel	Stationary kernel
boston	DT	mae	-1.15e+03	-6.96e+02
	MLP-adam	mae	-2.91e+02	-1.37e+02
	MLP-sgd	mae	-2.80e+06	-8.25e+10
	RF	mae	-3.93e+03	-6.09e+03
	SVM	mae	-3.30e+02	-1.47e+03
	ada	mae	-4.84e+04	-9.13e+04
	kNN	mae	-3.69e+04	-3.68e+04
	DT	mse	-1.91e+04	-2.53e+02
	MLP-adam	mse	-4.80e+05	-1.28e+03
	RF	mse	-1.44e+07	-1.88e+04
	SVM	mse	-6.59e+02	-4.53e+03
	kNN	mse	-1.11e+07	-9.94e+06

Table 7. Non-stationarity test on tasks involving `Diabetes` dataset

Dataset	Model	Metrics	Nonstationary kernel	Stationary kernel
diabetes	DT	mae	-1.58e+02	-3.39e+02
	MLP-adam	mae	-3.05e+04	-4.40e+02
	MLP-sgd	mae	-2.01e+05	-1.03e+03
	RF	mae	-2.26e+04	-1.15e+04
	ada	mae	-3.13e+04	-4.65e+04
	kNN	mae	-2.46e+06	-2.34e+06
	DT	mse	-1.51e+04	-1.03e+04
	SVM	mse	-5.14e+02	-2.39e+02

Table 8. Non-stationarity test on tasks involving `Digits` dataset

Dataset	Model	Metrics	Nonstationary kernel	Stationary kernel
digits	DT	acc	-6.75e+02	-1.02e+03
	MLP-adam	acc	-2.38e+02	-3.39e+02
	MLP-sgd	acc	-8.02e+04	-2.98e+02
	RF	acc	-4.53e+02	-1.50e+03
	SVM	acc	1.43e+02	-7.92e+00
	ada	acc	-1.17e+11	5.89e-01
	kNN	acc	1.41e+02	1.07e+02
	lasso	acc	-1.11e+01	1.05e+02
	linear	acc	2.68e+01	9.78e+01
	DT	nll	-6.52e+03	-1.55e+03
	MLP-adam	nll	-1.25e+02	-2.33e+02
	MLP-sgd	nll	-2.65e+02	-1.32e+02
	RF	nll	-1.82e+02	-6.96e+02
	ada	nll	-1.87e+05	-8.71e+00
	kNN	nll	-2.08e+03	-2.09e+03
	lasso	nll	-4.82e+01	-4.07e+02
	linear	nll	-3.72e+03	-3.48e+03

Table 9. Non-stationarity test on tasks involving Iris dataset

Dataset	Model	Metrics	Nonstationary kernel	Stationary kernel
iris	DT	acc	-1.03e+07	-1.93e+03
	MLP-adam	acc	-1.11e+07	-2.75e+02
	MLP-sgd	acc	-1.41e+04	-6.25e+02
	RF	acc	-2.00e+04	-9.08e+02
	ada	acc	-4.54e+13	2.01e+01
	kNN	acc	1.20e+02	8.05e+01
	lasso	acc	-1.29e+01	7.94e+01
	linear	acc	-5.91e+02	-8.76e+02
	DT	nll	-3.34e+07	-3.63e+02
	MLP-adam	nll	-1.62e+03	-1.90e+02
	MLP-sgd	nll	-9.69e+02	-2.21e+02
	RF	nll	-7.29e+03	-7.21e+02
	SVM	nll	-1.20e+02	-1.32e+01
	ada	nll	-3.21e+02	-1.15e+02
	kNN	nll	-7.26e+04	-7.26e+04
	lasso	nll	-4.11e+01	-4.13e+01
	linear	nll	9.68e-01	-1.63e+02

Table 10. Heteroscedasticity tests on tasks involving wine dataset

Dataset	Model	Metrics	Fligner Statistic	Fligner p-value	Levene Statistic	Levene p-value
wine	DT	acc	127.3	6.912e-09	3.553	7.195e-13
	MLP-adam	acc	85.37	9.945e-04	1.874	5.544e-04
	MLP-sgd	acc	109	1.845e-06	2.48	5.701e-07
	RF	acc	128.5	4.717e-09	5.069	2.014e-21
	SVM	acc	28.73	0.9908	0.5136	0.9975
	ada	acc	156.6	3.527e-13	3.968	3.215e-15
	kNN	acc	37.67	0.8807	0.6869	0.9473
	lasso	acc	29.8	0.9862	0.5981	0.9859
	linear	acc	21.28	0.9998	0.3839	1
	DT	nll	349.2	6.614e-47	10.46	1.115e-48
	MLP-adam	nll	57.19	0.1971	1.21	0.1646
	MLP-sgd	nll	110.1	1.362e-06	2.597	1.380e-07
	RF	nll	258	3.660e-30	6.468	4.597e-29
	SVM	nll	57.18	0.1975	1.006	0.4663
	ada	nll	152.8	1.323e-12	3.072	3.555e-10
	kNN	nll	178.2	1.410e-16	5.446	1.635e-23
	lasso	nll	83.94	1.394e-03	1.782	1.416e-03
	linear	nll	185.8	8.404e-18	5.01	4.312e-21

Table 11. Heteroscedasticity tests on tasks involving `breast` dataset

Dataset	Model	Metrics	Fligner Statistic	Fligner p-value	Levene Statistic	Levene p-value
breast	DT	acc	97.79	4.302e-05	4.62	6.650e-19
	MLP-adam	acc	133	1.113e-09	2.939	1.923e-09
	MLP-sgd	acc	116.8	1.854e-07	2.469	6.495e-07
	RF	acc	154.9	6.469e-13	6.661	4.353e-30
	SVM	acc	20.7	0.9999	0.3995	0.9999
	ada	acc	272.5	9.178e-33	13.57	6.582e-62
	kNN	acc	33.16	0.9596	0.5519	0.9941
	lasso	acc	20.78	0.9999	0.4291	0.9998
	linear	acc	21.15	0.9998	0.4545	0.9995
	DT	nll	260.5	1.280e-30	9.52	2.294e-44
	MLP-adam	nll	166.6	1.008e-14	3.643	2.247e-13
	MLP-sgd	nll	141.2	7.115e-11	2.669	5.661e-08
	RF	nll	185.8	8.495e-18	7.553	1.013e-34
	SVM	nll	76.98	6.526e-03	1.707	2.970e-03
	ada	nll	142	5.458e-11	4.283	5.274e-17
	kNN	nll	125.7	1.155e-08	4.337	2.635e-17
	lasso	nll	71.41	0.02	1.011	0.4565
	linear	nll	18.55	1	0.2714	1

Table 12. Heteroscedasticity tests on tasks involving `boston` dataset

Dataset	Model	Metrics	Fligner Statistic	Fligner p-value	Levene Statistic	Levene p-value
boston	DT	mae	73.51	0.01327	1.752	1.900e-03
	MLP-adam	mae	336.3	1.737e-44	14.4	3.611e-65
	MLP-sgd	mae	272.6	8.694e-33	6.561	1.480e-29
	RF	mae	28.79	0.9906	0.6768	0.9537
	SVM	mae	48.08	0.5106	0.9612	0.5508
	ada	mae	218.7	2.692e-23	13.59	5.542e-62
	kNN	mae	33.15	0.9597	0.619	0.98
	lasso	mae	30.4	0.983	0.6091	0.983
	linear	mae	16.17	1	0.251	1
	DT	mse	60.75	0.1211	1.33	0.07387
	MLP-adam	mse	387	4.504e-54	15.32	1.147e-68
	MLP-sgd	mse	353.2	1.185e-47	8.239	3.548e-38
	RF	mse	35.59	0.9242	0.8985	0.6692
	SVM	mse	25.01	0.9983	0.4491	0.9996
	ada	mse	249.1	1.398e-28	14.4	3.682e-65
	kNN	mse	27.75	0.9938	0.8247	0.7951
	lasso	mse	31.38	0.9764	0.5397	0.9955
	linear	mse	16.67	1	0.1726	1

Table 13. Heteroscedasticity tests on tasks involving `diabetes` dataset

Dataset	Model	Metrics	Fligner Statistic	Fligner p-value	Levene Statistic	Levene p-value
diabetes	DT	mae	56.52	0.2146	1.131	0.2601
	MLP-adam	mae	74.64	0.01059	2.573	1.847e-07
	MLP-sgd	mae	191.3	1.062e-18	17.87	8.498e-78
	RF	mae	79.38	3.898e-03	1.558	0.01174
	SVM	mae	2.436	1	1.810e-04	1
	ada	mae	179.8	7.883e-17	7.542	1.154e-34
	kNN	mae	67.48	0.04106	2.101	4.747e-05
	lasso	mae	176.2	2.950e-16	4.75	1.225e-19
	linear	mae	206	3.792e-21	5.714	5.490e-25
	DT	mse	44.52	0.6551	0.8264	0.7925
	MLP-adam	mse	100.4	2.109e-05	3.582	4.951e-13
	MLP-sgd	mse	202.9	1.257e-20	14.31	7.960e-65
	RF	mse	37.1	0.8938	0.8063	0.8224
	SVM	mse	4.004	1	4.740e-04	1
	ada	mse	189	2.510e-18	7.348	1.138e-33
	kNN	mse	88.62	4.545e-04	2.964	1.407e-09
	lasso	mse	257.6	4.341e-30	10.86	1.637e-50
	linear	mse	278.2	8.540e-34	10.01	1.216e-46

Table 14. Heteroscedasticity tests on tasks involving `digits` dataset

Dataset	Model	Metrics	Fligner Statistic	Fligner p-value	Levene Statistic	Levene p-value
digits	DT	acc	205	5.670e-21	14.29	9.219e-65
	MLP-adam	acc	256.7	6.239e-30	7.342	1.219e-33
	MLP-sgd	acc	210	8.188e-22	6.53	2.167e-29
	RF	acc	184.3	1.458e-17	15.61	9.379e-70
	SVM	acc	91.72	2.093e-04	2.187	1.790e-05
	ada	acc	99.34	2.832e-05	2.305	4.601e-06
	kNN	acc	35	0.9343	0.7042	0.9349
	lasso	acc	22.97	0.9994	0.4292	0.9998
	linear	acc	17.3	1	0.2963	1
	DT	nll	249.6	1.140e-28	15.71	3.892e-70
	MLP-adam	nll	339.8	3.816e-45	6.882	3.012e-31
	MLP-sgd	nll	244.8	7.740e-28	6.104	4.129e-27
	RF	nll	144	2.791e-11	7.435	4.059e-34
	SVM	nll	4.373	1	0.06091	1
	ada	nll	135.1	5.444e-10	3.294	2.061e-11
	kNN	nll	108.2	2.326e-06	3.059	4.211e-10
	lasso	nll	88.4	4.799e-04	2.116	3.995e-05
	linear	nll	103	1.024e-05	3.328	1.335e-11

Table 15. Heteroscedasticity tests on tasks involving *iris* dataset

Dataset	Model	Metrics	Fligner Statistic	Fligner p-value	Levene Statistic	Levene p-value
iris	DT	acc	207.1	2.440e-21	6.523	2.355e-29
	MLP-adam	acc	83.81	1.436e-03	1.838	7.989e-04
	MLP-sgd	acc	68.52	0.03413	1.409	0.04082
	RF	acc	155.5	5.311e-13	6.138	2.726e-27
	SVM	acc	198.4	6.990e-20	3.345	1.065e-11
	ada	acc	155.7	4.788e-13	5.018	3.858e-21
	kNN	acc	55.68	0.2378	1.124	0.2701
	lasso	acc	19.72	0.9999	0.4045	0.9999
	linear	acc	106.4	3.965e-06	2.959	1.502e-09
	DT	nll	322.2	7.375e-42	6.118	3.506e-27
	MLP-adam	nll	106.3	4.070e-06	3.123	1.869e-10
	MLP-sgd	nll	155.6	4.966e-13	6.386	1.264e-28
	RF	nll	321.3	1.066e-41	8.339	1.136e-38
	SVM	nll	188.4	3.217e-18	4.736	1.470e-19
	ada	nll	74.04	0.01194	1.414	0.03938
	kNN	nll	212.6	2.863e-22	8.838	4.118e-41
	lasso	nll	45.45	0.6177	0.5045	0.998
	linear	nll	36.64	0.9037	0.733	0.9101